PARAMETRIC OPTIMIZATION OF SLURRY EROSION IN PIPELINE MATERIALS USING FUZZY LOGIC AND ARTIFICIAL NEURAL NETWORKS

A

THESIS

Submitted in partial fulfillment of requirements for the award of degree of

Master of Engineering (M.E)

In

Thermal Engineering

Submitted by

ZUBIN MISHRA

(Roll No. 801383028)

Under the guidance of

Dr. SATISH KUMAR
Assistant Professor, MED
Thapar University, Patiala

Dr. S.K MOHAPATRA
Senior Professor and HMED
Thapar University, Patiala

MECHANICAL ENGINEERING DEPARTMENT

THAPAR UNIVERSITY, PATIALA – 147004

JULY 2015

CERTIFICATION

I, Zubin Mishra, declare that this thesis report entitled **"*Parametric Optimization of slurry erosion in pipeline material using Fuzzy Logic and Artificial Neural Networks*"**, submitted towards fulfillment of the requirements for the award of Master's Degree in Thermal Engineering, in Mechanical Engineering Department of Thapar University, Patiala, is entirely my own work. This document has not been submitted for any degree in any other institution.

Date: 15-07-2015
Place: Patiala

Zubi-
Zubin mishra
801383028
Thapar University, Patiala

This is to certify that above statement made by the candidate is correct and true to the best of my knowledge.

Dr. Satish Kumar
Assistant Professor, MED
Thapar University, Patiala

Dr. S.K Mohapatra
Senior Professor and HMED
Thapar University, Patiala

Countersigned by

Dr. S.K. Mohapatra
Senior Professor and Head
Mechanical Engineering Department
Thapar University, Patiala

Dr. S.S. Bhatia
Dean
Academic Affairs
Thapar University, Patiala

ACKNOWLEDGEMENT

First of all, I would like to express my gratitude to Dr. Satish Kumar, Assistant Professor and PG coordinator at Thapar University, Patiala for his patience guidance and support throughout this report. I am truly very fortunate to have the opportunity to work with him. I found his guidance to be extremely valuable.

I also express my special thanks to Dr. S.K Mohapatra, Senior Professor and Head of the Mechanical Engineering Department, Thapar University, Patiala providing me opportunity to conduct this work and bring it out in present from.

Last but not the least; I want to convey my heartiest gratitude to my parents and my friends for their immeasurable lobe, support and encouragement.

Zubin mishra

ABSTRACT

Wear is most common problems encountered in industries like thermal power plants. More than 51% of India's energy is met through large coal reserves. Coal combustion in thermal power plant generates nearly 20-25 % bottom ash. Bottom ash generated by thermal power plant is usually transported to ash ponds via mild steel pipelines. Many researchers have studied the effect of various operating parameters on the slurry erosion behavior of Mild steel using different environmental conditions.

The present work deals with the parametric study of erosion wear on coated and uncoated ferrous material in solid-liquid mixture. Erosion wear of Al_2O_3 + 13% TiO_2 coated Mild steel, SS202 and grey cast iron is investigated using slurry pot tester. Atmospheric Plasma Spraying is used to deposits ceramic coatings on the base material. Erosion wear at three different speeds 700rpm, 1100rpm and 1400rpm is evaluated at 25% and 45% slurry concentrations. The effect of two different particle sizes of 75μm and 250-350μm has also been investigated. The erosion mechanism shown by coated specimen was brittle in nature with grain pull out, grain boundary dislodgment and brittle fracture as major mechanism. Fuzzy logic and Artificial Neural Networks (ANN) has been implemented for predicting the erosion wear. ANN model is based on the database obtained from the experiments and involves training, testing and prediction protocols. The results predicted by ANN were more accurate than Fuzzy logic with average percentage error less than 5 %.

CONTENTS

Chapters	Title	Page No.
	CERTIFICATION	i
	ACKNOWLEDGEMENT	ii
	ABSTRACT	iii
	TABLE OF CONTENT	iv
	LIST OF FIGURES	vi
	LIST OF TABLES	vii
	NOMENCLEATURE	viii
Chapter 1	INTRODUCTION	1-8
1.1	Wear	1
1.2	Mechanism of wear	1
1.2.1	Erosive wear classification	3
1.3	Factors affecting erosion rate	4
1.4	Wear testing machines or tribometers	4
1.4.1	Miller testing apparatus	4
1.4.2	Slurry pot tester	5
1.4.3	Jet Impingement tester	5
1.4.4	Pin-on disk Apparatus	5
1.5	Surface coating method	6
1.5.1	Types of surface coating which include solid state	6
1.5.2	Types of surface coating which include liquid state	7
1.5.3	Types of surface coating which include vapour state	8
1.6	Future trends in surface coatings against wear	8
Chapter 2	Literature Review	9- 18
2.1	Erosion wear with or without coating	9
2.2	Erosion wear prediction using Taguchi method	16
2.3	Optimization using ANN	18
Chapter 3	Materials and coating method	19-26

3.1	Base material	19-21
3.2	Bottom Ash	21
3.3	Chemical Composition of material used	22
3.4	Microhardness	23
3.5	Coating powder	24
3.6	Coating Deposition	24
3.6.1	Thermal Spray Coating	25
Chapter 4	Experimental and results	27-40
4.1	Slurry pot tester	27
4.2	Preparation of slurry	28
4.3	Specimen	29
4.4	Experimental Parameters	29
4.5	Effect of rotational speed on the erosion rate	30
4.6	Effect of concentration of bottom ash on erosion rate	33
4.7	Effect of particle size on erosion rate	36
4.8	Erosion Mechanism	37
Chapter 5	Optimization of parameters using Fuzzy and ANN	41-55
5.1	Introduction	41
5.2	Principles of fuzzy logic	42
5.3	Algorithms used in fuzzy logic	43
5.4	Artificial neural networks	49
5.4.1	Basic concept of neural networks	49
5.4.2	Learning methods for ANN	54
Chapter 6	Conclusions and Future scope	
6.1	Conclusions	56
6.2	Scope for Future work	56

LIST OF FIGURES

Figure No.	Description	Page No.
3.1	Scanning electron microscope and Energy-dispersive spectroscopy of bottom ash	22
3.2	Scanning electron microscope and Energy-dispersive spectroscopy of bottom ash	24
4.1	Ducom Pot Tester	27
4.2	Slurry Pot	28
4.3	Dimensions of specimen used	29
4.4	Weight loss (Cw=25 %) at 90 min	31
4.5	Weight loss (Cw=25 %) at 180 min	31
4.6	Weight loss (Cw=50 %) at 90 min	32
4.7	Weight loss (Cw=50 %) at 180 min	32
4.8	Relative erosion of mild steel at 90 min	33
4.9	Relative erosion of mild steel at 180 min	34
4.10	Relative erosion of grey cast iron at 90 min	34
4.11	Relative erosion of grey cast iron at 180 min	35
4.12	Particle Size on erosion rate	36
4.13	SEM micrograph of coated mild steel with erodent size 250-350μm	37
4.14	SEM micrograph of coated mild steel with erodent size 75μm	38
4.15	SEM micrograph of mild steel at 90 min	39
4.16	SEM micrograph of mild steel at 180 min	40
5.1	Structure of fuzzy system	42
5.2	Mamdani Fuzzy Interference System	43
5.3	3-D Surface Plot for erosion rate with speed concentration and time for mild steel	45
5.4	3-D Surface Plot for erosion rate with speed concentration and time for SS202	47
5.5	Artificial neural network model	49
5.6	Neural network	51
5.7	Graph between experimental and predicted values	55

LIST OF TABLES

Table No.	Description	Page No.
3.1	Chemical composition of Mild steel, Grey cast iron and SS202	22
3.2	Hardness value of uncoated base material	23
3.3	Hardness value of coated base material	23
3.4	Comparison of different Thermal Spray coating	25
3.5	Operating parameters of Atmospheric Plasma Spraying (APS)	26
4.1	Experimental parameters and specification	29
5.1	Fuzzy rules	44
5.2	Defuzzification Algorithms	44
5.3	Experimental and fuzzy prediction for uncoated mild steel	45
5.4	Experimental and fuzzy prediction for coated mild steel	46
5.5	Experimental and fuzzy prediction for uncoated SS202	46
5.6	Experimental and fuzzy prediction for coated SS202	47
5.7	Experimental and fuzzy prediction for uncoated SS304	48
5.8	Experimental and fuzzy prediction for coated SS304	48
5.9	Actual values for input and output variables	53
5.10	Normalized value for input and output variables	53
5.11	Percentage error between Experimental and ANN model	54

NOMENCLATURE

H_v	Hardness value
lpm	Litres per minute
C_w	Slurry concentration
RPM	Rotation per minute
α	Velocity exponent
γ	Concentration exponent
μ_A	Membership function
U	Result of defuzzification
u	Output variable
min	Lower limit for defuzzification
max	Upper limit for defuzzification
inf	Smallest value
sup	Largest value
Φ	Activation function

CHAPTER 1 INTRODUCTION

1.1 WEAR

Wear is characterized as a procedure of losing material from surfaces which have been rubbed against one another. Relative movement between machine surfaces practically prompts an adjustment in these surfaces and it leads to some type of mass loss from the surface. Wear relies on material properties like hardness, quality, pliability, work solidifying and so forth. Wear can be classified as:

- Adhesion
- Abrasive
- Erosion
- Fatigue
- Chemical Wear

1.2 MECHANISMS OF WEAR

Industries should particularly avoid wear as this leads to loss of potential and functionality of the component. Some industries require wear where material removal rate is of prime importance such as manufacturing sector. Wear rate depends on friction and its almost related to it. But the relation between wear and friction inside the contact surface is quite complex and it is not well understood. Many researchers assume that low friction leads to low wear and vice versa which is not universally accepted.

- **Sliding wear:** Sliding wear results from the adhesive contact between two surfaces. There are basically two types of sliding wear Scoring and galling. Scoring occurs when there is a lubricated contact between surfaces while Galling occurs with dry friction of low sliding speed. In both types of phenomena there is some localized welding and material transfer. The main

theory for sliding wear of metals is based on the assumption that contact between two surfaces occurs where asperities contact and the local deformation is plastic. The true contact area is therefore given by the summation of individual asperity contact areas and is closely proportional to the normal load. Sliding wear occurs due to two or three different mechanisms. In first the oxide control of the sliding wear along with low wear rates are experienced at high temperature because oxide growth takes place at high temperature. Sometimes oxide debris leads to abrasive wear of the surface along with sliding wear which leads to new types of wear known as Fretting wear. The second mechanism occurs due to high contact stresses which breaks the oxide films and there is actual metal to metal contact which leads to cold welding and when there is relative movement between surfaces which results in fracture of small pieces from the surface. Wear caused by this mechanism leads to galling. Third mechanism occurs due to cyclic stresses generated by the pressing of one surface on the other surface.

- **Abrasive wear:** There are two types of abrasion: grooving abrasion and rolling abrasion. Grooving abrasion causes more material loss as compared to rolling abrasion. Abrasive wear is considered to be the major contribution of wear in industries. Abrasive wear occurs due to sliding of embedded solid particles inside the surface under the action of some external force. There are three different mechanisms which lead to abrasive wear namely plowing and cutting. Plowing leads to displacement of material away from the abrasive particles results in formation of grooves. The displaced material surrounds the groove which gets removed by subsequent collision with the abrasive particles. Cutting occurs due to micro chipping of the material from the surface under the impact of abrasive particles which resembles the conventional machining process.

- **Erosive Wear:** Erosion Wear is a phenomenon in which small hard particles striking the surface at various angle leads to removal of material or causing damage to it. For Example Turbine blades, pump impellers etc. But in some applications erosion wear is beneficial like cleaning and surface preparation for coating by grit blasting and cutting through rocks or subsea steel oil structures using abrasive water jets.

1.2.1 Erosive wear is further classified into two categories

- Liquid-droplet erosion
- Solid-particle erosion

- **Liquid-droplet erosion:** Damage of target particle under the continuous impact of liquid droplet is defined as Liquid-droplet erosion. The problem of liquid-droplet is encountered in high speed aircrafts, missiles and steam turbines. The liquid-solid droplet velocity is dependent on impact velocity and the radius of droplet. The response of brittle materials under liquid impact leads to generation of cracks surrounding the area. The cracks generated in the form of discontinuous annular rings which results in material removal from the surface. The behavior of ductile metals is somewhat different from the response given by brittle materials. In ductile material due to impingement of liquid droplet there is suppression of metal at the centre while the outer edge gets raised.

- **Solid-particle erosion:** Loss of material under the impact of hard particles on the solid surface is called as Solid-particle erosion. The carrier medium for solid particle can be either gas or liquid. A pipeline dealing with slurry transportation regularly faces the problem of solid-particle erosion. Archard law predicted that erosion rate is inversely proportional to the hardness of the material but experimental results proved that it’s inversely proportional to square of hardness value.

1.3 FACTORS AFFECTING EROSION RATE

Many variables are known to affect erosion rate. It is possible to control one or several factors but material properties and particle shape is difficult to quantify.

- **Velocity** According to basic theory of wear volume of material removal from the surface is directly proportional to distance travelled by the particle multiplied by normal force. Previous researchers observed that volume removal is proportional to velocity with power of n which varies from 1 to 3.5 **(Truscott, 1975).** The value of n depends on various wear mechanisms and type of slurry used.
- **Concentration** Many researchers have studied the effect of slurry concentration on the erosion rate and they concluded that correlation between the erosion rate and concentration is non linear in nature.
- **Particle size** increase in particle size increases the erosion rate but the correlation in not universally accepted. **(Soo, 1967)** observed that the erosion rate depends on the collision efficiency which is defined as the number of particles striking per unit area. The collision efficiency increases with particle diameter.

1.4 WEAR TESTING MACHINES OR TRIBOMETERS

Wear testing machines are used to assess the erosion or displacement of solid surface under the impact of another surface or particle. Wear testing helps to determine the workability of the sample or specimen which is going to be used in industries. Testing can be performed under various environmental conditions to simulate actual working scenarios.

1.4.1 Miller testing apparatus (ASTM G-75)

Miller testing apparatus is based on the procedure given under ASTM G-75 standard. The Miller number is used to rank the abrasiveness of slurries in terms of wear of standard reference manual. Slurry Abrasive response of material (SAR number) is an index to determine the abrasive response of different material under slurry conditions.

1.4.2 Slurry pot tester (ASTM G73-83)

This test apparatus is little in size, basic in outline, simple to work, practical and can be utilized to create trial information at a quickened rate. In this test apparatus, the wear specimen are pivoted in a cylinder shaped pot containing strong fluid mixture. The specimen is hold on to a fixture associated with pivoting steel shaft. The propeller having two razor sharp edges toward the end joined with a turning shaft keeps the hard particles suspended in a fluid. The relative movement between the wear samples with slurry causes disintegration wear. Impact of different working parameters like fixation, speed and effect edge can be effectively calculated.

1.4.3 Jet Impingement tester (ASTM G73-82)

In this experimental procedure the solid specimen is continuously eroded by the impact of liquid jet. This test is performed for the evaluation of corrosion behaviour of specimen. In this method water is sprayed through the nozzle on to the solid specimen. It comprises of a pump and an ejector to issue a jet through a nozzle. Jet impingement tester simulates the wear for direct impact of solid particles in equipment such as pumps, bends, tee junctions, elbows, contractions etc. This method is not applicable for predicting erosion wear or particle impact in bouncy flows.

1.4.4 Pin-on disk Apparatus (ASTM G99)

This method measures the wear rate of materials using pin-on-disk apparatus. This method also helps in determining the coefficient of friction. During this tribological test, the pin rotates against a stationery disk under constant load. The amount of wear is determined by measuring appropriate linear dimensions of both specimens before and after the test, or by weighing both specimens before and after the test.

1.5 SURFACE COATING METHOD

A coating is a covering that is applied to the surface of an object, usually referred to as the substrate. Surface modification is further classified into three groups:

First group consists of those processes which modify the outer surface but does not change the chemical composition of the substrate for example shot peening and surface remelting. Second group consists of process which changes the chemical composition of the surface for example carburizing and hardening. Third group consists of processes which add some new material using Chemical Vapor Deposition, Physical Vapor Deposition and High Velocity Oxy-Fuel etc.

Surface coating is divided into three categories:

- Types of Surface coating which include solid state
- Types of Surface coating which include liquid state
- Types of Surface coating which include vapour state

1.5.1 Types of surface coating which include solid state

- **Friction Surfacing:** It is a solid state technology used to deposits dissimilar material on to the surface using a depositing tool. Resulting coatings are relatively flat and are commonly deposited to a thickness between 0.5 and 3 mm depending upon operating parameters and materials. The coating thickness depends on the relative movement between the specimen and the depositing tool. The metal is deposited by the lateral movement of specimen and the heat generated at the tip of the rod. The temperature and pressure environment leads to diffusion process between the deposited material and the specimen. Since no bulk melting takes place it easy to join two different materials. Lower heat input results in less heat affected zone which prevents degradation of materials. Its key advantages include high energy efficiency and low impact on environment.

- **Kinetic metallization and cold spray:** Cold spray is a process in which solid particles are accelerated to supersonic speed in order to collide them with substrate which is to be coated. The high speed of the particle creates a

metallurgical bond between the particles and the substrate. Since this process occurs at low temperature, the physical properties of powder before and after deposition remain almost same. Helium or nitrogen is used as a carrier gas. Cold spray process is not suitable for brittle materials like ceramics. Velocity greater than critical velocity will leads to deposition of coating. The critical velocity depends upon the spray material and it's also affected by particle size and impact angle.

1.5.2 Types of Surface coating which include liquid state

- **Thermal Spraying:** It is a process in which the powder metal is first heated to form molten droplets and then they accelerated towards the substrate and upon impact its solidfy and get deposited. The energy required for melting either comes from combustion of fuel or from electrical supply (arc or plasma). Thermal spraying always involves high velocity as this leads to better porosity in the coating substrate. The thickness of the coating is limited by the thermal stress developed inside the coating. The thickness of coating varies from 100μm to 500μm.

- **Weld hard facing:** Depositing of hard material on the surface of the substrate using various welding processes like GMAW, GTAW and SAW etc is defined as weld hard facing. Weld hard facing tends to be brittle and susceptible to cracking. In weld hard facing the surface of the substrate which is to be coated also gets melted and forms a strong metallurgical bond between substrate and the coating. It is used where the component is subjected to abrasive wear. The thickness varies from 1mm to 50 mm.

- **Laser cladding:** In this method, a powder from which the coating is to be formed is melted by a laser. Traditionally, CO2, neodymium-doped yttrium aluminium garnet (Nd: YAG) and excimer lasers have been employed although more recently high-powered diode lasers have been used. Laser-clad coatings are typically between 0.5 and 3 mm in thickness and exhibit the high bond strengths associated with fusion bonding with the substrate.

1.5.3 Types of Surface coating which include vapour state

Physical vapour deposition

It is a collective set of processes which adds material on the surface whose thickness varies from few nanometers to micrometers. Three steps are required for deposition of material

- High temperature vacuum is required to vaporize the material from solid surface
- Transportation of vapours to solid surface in vacuum
- To generate thin films the vapours are condensate on the substrate

Chemical vapour deposition

If the ratio of width to depth known as aspect ratio is high then PVD cannot be used because it does not give good side wall coverage. Semi conductor industries often used CVD process for deposition of thin films. Chemical vapour deposition is a chemical process generally used for high purity less porosity and high performance materials. CVD process is highly expensive and always leaves by product which has to be removed by continuous gas supply.

1.6 FUTURE TRENDS IN SURFACE COATINGS AGAINST WEAR

Newer methods of coating techniques, materials etc are being applied in order to improve the properties of the substrate and also to minimize cost of the component. The most important aspect of coating material is the hardness, higher hardness leads to lesser erosion wear rate. To improve the hardness value many coating design is based on the addition of some inclusions which hindered dislocation motion. Nanocomposite coatings are structures that contain nanosized features such as precipitates or fi lm layers.

CHAPTER 2 LITERATURE REVIEW

2.1 EROSION WEAR WITH OR WITHOUT COATING

Grewal et al. (2013) studied the effect of velocity, impact angle and concentration on the erosion mechanism of CA6NM turbine steel. Non- recirculationg type erosion tester was used for conducting experiment. The maintained Stand of distance (SOD) between nozzle and sample was around 20mm. At low velocity erosion rate is inversely proportional to concentration but at high velocity its changes its trend showing direct relation between erosion and concentration. This shows that there is some interaction between velocity and concentration. From line plots degree of interaction between velocity and concentration was found to be more evident than the interaction between velocity and impact angle. From contour diagrams they observed that velocity has the most significant impact on erosion compared to impingement angle. At different impingement angle diverse types of erosion mechanism has been observed, platelet mechanism was noticed at 90^0 impact angle and at 30^0 angle mixed cutting and ploughing mechanism was found to be the most dominant erosion mechanism. .

Grewal et al. (2013) evaluated the performance of CA6NM turbine steel with Ni-Al_2O_3 composite coating subjected to slurry erosion conditions. Nickel powder under SEM showed spherical morphology while aluminum oxide showed irregular and blocky appearances. For conducting experiment ASTM G 73 standard procedure was used. To evaluate the effect of Al_2O_3 on erosion behaviour of composite, different proportion of Al_2O_3 in the range of 20%, 40% and 60% by weight was mixed with Nickel powder. The effect of velocity was considered at two different speed of 4m/s and 16m/s. Surface Roughness and porosity showed direct relationship with the percentage of alumina content in the coating. Composite with 40% of Al_2O_3 exhibited better resistance towards erosion as compared to 20% and 60%. The effect of velocity on erosion rate was maximum in case of 60% and minimum in 40% of Al_2O_3. Brittle mode of erosion was exhibited by all three Ni based coating. The erosion mechanism was not affected by time due to similar surface morphology observed at varying time. Primary erosion mechanism consists of cracking, removal of splats, fracture of matrix

and spalling of coating. Main parameter to control erosion resistance was fracture toughness of coating material.

Torres et al. (2013) analyzed the erosion performance of AISI 420 Stainless Steel. They used angular silicon carbide and spherical round grit particles as an erodent material. Jet impingement tester was used for conducting experiment. The particle size of erodent was varied from 400 to 420μm with impact angle varying from 30^0 to 90^0 with an interval of 15^0. The particle velocity for both types of erodent was 24 m/s. After performing experiment they observed that erosion caused by spherical round grit was comparatively less as compared to angular silicon carbide. Wear scar was observed to be elliptical at 30^0 and circular at 60^0. The maximum erosion occurs at 30^0 impact angle which confirms that the material is exhibiting ductile behavior. It was identified later that wear mechanism predominantly consists of pitting and plowing action, formation of flakes and wear ripples.

Andrews et al. (2014) conducted a series of experiment to study the effect of impact angle on the slurry erosion behaviour of Stellite 6 and SS316. Stellite 6 was manufactured using two process namely lost wax casting and sand casting. They observed that Cobalt rich dendrites structure were present under both manufacturing process. The performance of both the material was evaluated using recirculating impingement jet apparatus. The angles taken for erosion study were 45^0 and 60^0. They observed that mass loss for stainless steel decreases from 45^0 impact angle to 60^0 which suggest ductile behavior. While in case of Stellite 6 the mass loss is same at 60^0 which lead to a conclusion that the cast Stellite 6 has a ductile matrix but due to the presence of brittle networks of chromium the mass loss appears to be more at higher impact angle. The scar at low angle appears to be elongated due to the particle abrading on the surface of the specimen. At low impact angle sliding mechanism was observed to be most dominant mode of erosion. They also concluded that greatest scar depth appears to be in direct correlation with the maximum mass loss.

Elrhman et al. (2014) studied the influence of carburizing on the erosion behavior of AISI 5117 using whirling arm-test rig. Silica sand was used as an erodent with size varying from 250-355 μm. The impact velocity was 15 m/sec with particle concentration of 1% by weight. To analyse the effect of impact angle four different angles of 30^0,45^0,60^0 and 90^0 were used. Case depth obtained from carburizing at 6h and 12h was found to be 0.65mm and 0.90mm respectively. The erosion resistance increases by 70% and 74 % at impact angle of 30^0 when carburizing was done at 6h and 12h respectively. SEM micrographs at 6h showed martensitic with retained austenite on the outer surface of the specimen while at 12h it was observed that martensitic content increases due to high carbon content. Maximum mass loss appears to be at 45^0 impact angle. Due to normal resolved component at higher impact angle the erosion mechanisms changes from microcutting at lower angle to extrusion and micro-forging. They observed that mass loss of carburized specimen is inversely proportional to the case depth and surface hardness of the carburized substrate. The reasons behind low erosion rate of carburized specimen as compared to untreated steel substrate is due to the presence of large number of carbides which prevent the propagation of cracks in the carburizing layer.

Gandhi et al. (2014) investigated the effect of Cobalt free laser cladding on the erosion resistance of SS316. To evaluate the performance of cavitation and slurry erosion Metco-41C and Colmonoy-5 were chosen as the coating material. They used ultrasonic cavitation tester for experimental studies. Due to the presence of molybdenum in Metco-41C, it exhibit high impact resistance and tensile strength. Particle size of coating powder varies from 45-106 μm. Concentration of slurry used in the experiment was around 20%. They observed that Metco-41C hypo eutectoid composition of alloy was formed due to the presence of fine dendrites and cells of Cr-Co solid solution in eutectic mixtures. Due to high cooling temperature during cladding, fine grain structure was present on the interface. They noticed that Colmonoy-5 showed higher cavitation erosion as compared to Metco-41C due to less toughness and work hardening ability of its micro constituents. The metallographic samples showed that the clad layers of Colmonoy-5 and Metco-41C primarily contain very fine columnar dendritic structure while clad-substrate interface exhibited planar and non-epitaxial mode of solidification in case of Colmonoy-5 deposits.

Goyal et al. (2014) studied the erosive wear of Cr3C2-NiCr coated ASTM A743 turbine steel under slurry erosion condition. They used high speed erosion test rig (TR401, Ducom, India) for conducting experiment. Two different particle sizes of 100 and 300μm were used. They observed that interface seems to have nearly a continuous contact of coating and substrate steel. Presence of irregular shaped projections on the surface suggested that it might be due to insufficient melting of the carbide particles. The apparent porosity of the coating was found to be less than 2%. The value of exponent α for velocity was observed to be 1.40 for the uncoated CA6NM steel and 1.20 for the HVOF sprayed Cr3C2–NiCr coating on CA6NM steel. They noticed that rebounding of impact particles from the target surface resulted in less value of exponent. The value of exponent β for particle size was found to be 0.47 for the uncoated CA6NM steel and 0.50 for the HVOF sprayed Cr3C2–NiCr coating on CA6NM steel. From line plots degree of interaction between particle size and concentration was found to be more evident than the interaction between velocity and concentration. Uncoated turbine steel exhibited ductile behaviour while coated steel exhibited brittle mode of fracture. Crater and lip formation was the most dominant mode of erosion followed by plastic deformation, cutting and plowing. While in case of coated substrate, the main mechanism was microchipping and localized chip formation.

Islam et al. (2014) analyzed the erosion attack on APIX42 pipeline steel under high abrasive feed rate. They performed erosion test using sand blast type test rig. They noticed that erosion rate depends on the impact angle at higher velocities. They investigated using particle velocity of 36m/sec, 47m/sec, 56m/sec and 81m/sec at impingement angle of 30^0,45^0,60^0 and 90^0 respectively. They observed that at impact angle of 30^0 the erosive scar appears to be elliptical in shape due highly diffuse particle stream. But at higher impact angle of 90^0 the scars appears to change its shape from elliptical to circular. The erosion rate is minimum at impact angle of 90^0 due to the colliding between the incoming particles and the rebounding particles and there might be some reinforcement of erodent on to the surface of the specimen. They observed that the vertical component of velocity leads to penetration of the surface while the horizontal component of velocity squeeze the metal ahead of it to form ridges and causes the surface to flatten and gets fractured. They concluded that several

erosion mechanisms were responsible for erosive wear at high impact angle which includes embedding of erodent on the surface of specimen, heavy plastic deformation and particles interference.

Lotfollahi et al. (2014) investigated the effect of friction stir processing (FSP) on erosion- corrosion behaviour of nickel-aluminum bronze (NAB). A tool tilt angle of 3^o was used for all FSP operations. Erosion (E) and Erosion–Corrosion (E–C) experiments were carried out using a slurry jet impingement rig. The cast NAB is characterized by coarse microstructure, composition segregation, and shrinkage porosity, which decrease the mechanical properties and corrosion resistance of the NAB castings. In different rotation rates in FSP samples observed different microstructures on the upper surface of stir zone. It was observed that increasing hardness resulted in increased erosion rate which might be due decrease in strain hardening rate. The erosion corrosion rate increases by decreasing the impact angle. The highest erosion-corrosion rate was observed at impact angle of 30^0 which might be due to shear stress. The SEM image of the specimen surfaces showed that on cast sample surface plastic deformation mechanism was present and some signs of brittle fracture were added to previous mechanism on the FSP NAB samples.

Lindgren et al. (2014) analyzed the effect of erodent charactertics on wear behaviour of titanium using slurry pot tester. The erodent used is quartz with size varying from 100-600μm. Chromites, matte, ore, concentrate and tailings were used as other erodent material. The shape parameters were determined using SEM combined with INCA Feature image analysis software. No shape analysis of concentrate and ore could be identified due to their agglomeration. Tailings particles were having the highest aspect ratio. Chromites particles exhibited the lowest circularity value because they contained the greatest number of sharp corners. Due to very fine particle size concentrate showed less volume loss. Highest erosion rate was observed by quartz particle. SEM image confirmed that the quartz particles resulted in caters surrounded by lips on Stainless Steel due to its ductile behavior while on titanium surface it resulted in micro cutting. Testing of chromites on titanium showed deep penetration marks filled with fine erodent particles. They concluded that weight loss not only

depends upon the kinetic energy of the particles but also on the shape of the particles. Titanium Grade 2 showed slightly more erosion than stainless steel 316L.

Nguyen et al. (2014) conducted a series of experiment using a newly developed air-sand erosion tester which is capable of producing velocity greater than Mach 3. They investigated the effect of impact angle on the erosion behaviour of SUS304 at higher velocities. The range of angle varies from 10^0 to 90^0.The maximum erosion rate is achieved at impact angle of 40^0, after that erosion rate decreases due to more number of particles colliding with the rebounded particles which results in decreasing of erosion rate. At impact angle of 10^0, the erosion scars appears to be shallow groove which then suddenly changes to deep round holes at 90^0 impact angle. Depth of cut follows similar trend with erosion rate when the angle of impact changes from 10^0 to 90^0. The difference between air-sand erosion and water-sand erosion can be predicted by observing the scars. V shaped erosion features appear in air-sand erosion and W shaped appears in water-sand erosion. Surface roughness achieved its peak value at 40^0 impact angle similar to depth of cut. At very low impact angle micro-cutting appears to be the dominant erosion mechanism but as the impact angle increases erosion mechanism changed in nature from micro-cutting to indentation induced plastic deformation.

Wan et al. (2014) investigated the erosion behaviour of Ti(C,N)-based cermet using fabricated test rig. 5% by weight Al_2O_3 sand with size varying from 150-250μm was used. They analyzed the erosion mechanism of cermet under solid-liquid erosive conditions. EDS analysis showed that under erosive wear for 3hour the nickel content gradually decrease which suggest the binder loss is significant in later stages of erosion wear. Degradation charactertics for initial stage showed surface scratch, crack nucleation at interface and intergranular cracks propagation while at later stages of erosion there is grain fracture and fragments removal. Microcutting action of solid particles and loading impact of erodent are the dominating factor which leads to metal removal in solid-liquid erosive environment.

Andrews et al. (2015) investigated the erosion-corrosion mechanism of two cermets, zirconia and S31600 under solid-liquid impingement with silica sand at 20^0 and 90^0 impact angles. Application of cathodic protection and polarization were used to

investigate the chemical properties of the materials. SEM and 3-D optical Imaging were used to analyze the erosion mechanism exhibited by different materials under erosive-corrosive environment. Mass loss at 90^0 was several times greater than at 20^0 which confirmed that the behaviour shown by zirconia is brittle in nature. As compared to S31600 both cermets showed better erosion resistance due the higher hardness of WC-Co and WC-Ni. Due to the presence of nickel binder in WC-Ni cermet it showed overall the best erosion resistance as compared to other different materials. The shaped of the wear scar was U shaped for all testing material with zirconia showing deepest scar. Cathodic protection was insignificant in WC-Ni due to nickel binder susceptible to hydrogen embrittlement.

Lindgren et al. (2015) studied erosive wear of three duplex steel grades LDX2101, 2205 and 2507 and two stainless steel grades 316L and 904L. They took two quartz erodent with one being coarser and another being finer. The experiments were performed using impeller type slurry pot tester. The impeller blade has one pressure side and another suction side, each sample is fitted on both sides of the impeller. The pressure side faced more uniform erosion while due to high trailing vortices the suction side faced highly irregular erosion behaviour and more mass loss. Duplex steel grade showed better erosion resistance as compared to austenitic stainless steel grade due to higher hardness of duplex grade. Maximum mass loss was exhibited by 904L while LDX 2101 showed minimum mass loss. Wear marks of 316L showed the presence of embedded quartz particle due to lower hardness value. The surface roughness after the erosion test got smoothen due to impact of erodent particles, duplex grade steel showed more smoothening effect than austenitic stainless grades. The effect of particle on erosion rate at suction side was different from the pressure side due to the interaction effect between trailing vortices, tip speed and particle size. At the pressure side of the impeller highest mass loss was exhibited when the particle size was coarser and tip speed was maximum, but the influence of gaseous phase was found to be insignificant which suggested that erosion rate was independent of test temperature. The effect of test temperature was significant on the suction side of impeller due to interaction between the gaseous phase and the trailing vortices.

Ren et al. (2015) prepared SiC ceramic foam/epoxy composite and investigated the effect of different SiC foam on the erosion behaviour of the composite. SiC ceramic

foam/epoxy composite was prepared using solid phase sintering process using polymer foam replication method. Slurry performance of the specimen was investigated using rotating disk tester with specimen attached to the outer edge of the disk. Among four treatments of SiC ceramic foams, it is found out that fabricating a transition layer is an efficient method to improve the mechanical properties of Sic foam/EPs. The reinforcement of SiC foam to composities is better than dispersed SiC particles as this helps in preventing erosion and can be potentially applied under slurry erosion conditions.

2.2 EROSION WEAR PREDICTION USING TAGUCHI METHOD

Mahapatra et al. (2009) investigated the effect of three different particulate fillers on the wear charactertics of composite using Taguchi statistical method. E-glass fiber was used as a base material for investigation purpose. The composite variation was achieved using different proportion of Cement By-Pass Dust (CBPD), alumina particles and silicon carbide. Silicon carbide increases the hardness of the composite while alumina did not affect the hardness value. The addition of CBPD significantly increases the hardness value but this hardness was achieved at 10% CBPD and after that there was little variation in the hardness value. The flexural strength of the composite increase with CBPD and alumina upto 10% CBPD but after that it shows decline trend. The effect of silicon carbide on flexural strength showed decline trend with increase in filler percentage. L27 orthogonal array was used for design of experiment, smaller is better charactertics was used for signal/noise ratio. In order to find the statistical variation analysis of variance was done using MINITAB 14. Addition of alumina particles showed better erosion resistance as compared to other particles. The sand of distance was found to be least significant factor while filler content, impingement angle and impact velocity was most significant variable which affected erosion rate.

Bagci et al. (2013) studied the addition of boric acid particles with two different variations on erosion performance of glass fiber reinforced epoxy resin using Taguchi method. They also investigated the interaction of solid particles on the erosion behaviour of the specimen. L36 orthogonal array with 35 degree of freedom was used

to design the experiment. Analysis of different parameters on erosion rate was performed using MINITAB 16 software. Addition of 30% boric acid particles improved the erosion performance of the material due to the formation of strong bond with epoxy. Maximum erosion rate was observed at 30^0 impact angle. Using ANOVA the percentage contribution of material was 52.61%.

Joshi et al. (2014) studied the effect of Al2O3 particles the erosion behaviour of glass/epoxy composites. Experiments were performed using taguchi method with L27 orthogonal array having 26 degree of freedom. From the line plots it was observed that interaction effect of speed and concentration was not as significant as the interaction between speed and impact angle. Using analysis of variance the percentage contribution was estimated which suggested that slurry concentration was most significant factor affecting the erosion rate followed by impact angle and speed. From regression plots the R squared value obtained was around 90% which confirmed that experimental data and the data obtained using developed model has a good correlation. The maximum value of erosion obtain using slurry test was at 60^0 impact angle. The addition of Al2O3 particles reduces the mass loss during experiment which confirms that with particle addition the crack propagation is hindered due to the barrier caused by the Al2O3 particles.

Sridhar et al. (2014) analyzed the effect of nanoclay loading in vinyl ester/glass composities using orthogonal array. The erosion tests were performed using ASTM G76 standard. L27 orthogonal array with 5 controlling factors has been used in this research work. The mean S/N ratio was found to -51.22 db. Minimum erosion was observed for combination of 3% nanoclay addition, impact angle 30^0, velocity is 66m/s, SOD is 120mm and erodent size of 420μm. The ductility of the composite is lost due to the addition of nano-clay which is brittle in nature. From the main plots it was observed that velocity and sand of distance (SOD) did not contribute significantly towards the erosion rate. The interaction between nano clay and SOD was found to be insignificant. Using analysis of variance it was observed that the effect of nano clay addition was the most important factor while the impingement velocity was found to insignificant

2.3 OPTIMIZATION USING ANN

Mishra et al. (2012) investigated the response of Metal Matrix Composite (MMCs) to the impingement of solid particle. Pretreated Al2O3 particles are reinforced into the molten ZA-27 in different weight proportions (0, 3, 6, and 9 wt %) with a continuous stirring action. An air-jet erosion tester is used to simulate the real time erosion situation. Dry silica sand of average particle size 450 μm is used as the erodent. Erosion trials are made as per the experimental design based on Taguchi's L16 orthogonal array. A prediction model based on artificial neural network (ANN) is used to predetermine the erosion rate at different operating conditions. They observed that the impact velocity is the most significant factor followed by the filler content whereas others have relatively less significance on the erosion wear rate of MMCs

Pati et al. (2013) predicted the erosion response of LD (Linz Donawitz) slag filled composite using artificial neural network (ANN). Epoxy LY 566 is used as a base material for manufacturing of composite. The solid particle erosion has been carried as per ASTM G76 standard. Composites of five different compositions (0, 7.5, 15, 22.5, 30 wt% of LD slag reinforced in epoxy resin) are prepared by simple hand lay-up technique .They used erodent particle with size ranging from 50 to 200μm with an interval of 50μm. L_{16} Orthogonal Array was used for conducting experiment.Significant process parameters predominantly influencing the rate of erosion are identified. Here, factors like impact velocity, LDS content, impingement angle and erodent temperature in declining sequence are found to be significant to minimize the erosion rate. The model is based on the database obtained from the experiments and involves training, testing and prediction protocols.

.

CHAPTER 3 MATERIALS AND COATING METHOD

In present study bottom ash used as an erodent was procured from Guru Gobind Singh Super Thermal power plant. Thermal Power Plant basically produces 20-25 % of bottom ash from each coal sample. Bottom ash is removed from the bottom of the boiler: wet and dry. Ash is either transported to ash ponds or dry disposal as ash mounds. Its concentration in the slurry ranges from 40-50% by weight. Wet disposal is the most common method for bottom ash disposal in India. During transportation there is particle degradation due to impact of abrasive bottom ash on the side walls of pipeline. The abrasive action of particles leads to volume loss of pipeline material used in slurry transport. Our basis of study is to investigate the effect of particle on the erosion behavior of ferrous sample and in order to improve erosion resistance the ceramic coating was deposited on the given ferrous substrate using thermal spraying technique.

3.1 BASE MATERIAL OR SUBSTRATE

The testing material which was used for our research purposes was mild steel 1015, grey cast iron and SS202.

Mild steel (1015)

Mild steel is an iron carbon alloy consisting of less than 0.25 % carbon. The less percentage of carbon makes it more ductile and has less hardness value. The application of mild steel is basically pipeline material and it’s unsuitable for structural work.

- It is utilized as a part of twisting and swaging procedures.
- Carburized parts that incorporate worms, riggings, pins, dowels, non-discriminating segments of hardware and pass on sets, instrument holders, pinions, machine parts, ratchets, dowels It is generally utilized for installations, mounting plates and spacers.

- It is suitably utilized as a part of utilizations that needn't bother with high quality of combination steels and high carbon.
- It gives high surface hardness and a delicate center to parts that incorporate worms, puppies, pins, liners, hardware parts, uncommon screws, wrenches, chain pins, oil device slips, tie bars, stay pins, studs and so on.
- It is utilized to enhance boring, machining, threading and punching procedures.

Grey cast iron (ASTM 40)

Grey cast iron is a type of cast iron which contains graphite flakes in its microstructure. Grey cast iron has higher strength in compression as compared to tension. Due to presence of graphite flakes its act as a brittle material. Its notch sensitivity is low but has high value of damping capacity, which helps in vibration absorber.

Application of grey cast iron:

- Class 300 Grey Iron: Can be used in producing heavy-duty machine tools, bed, presses, high pressure hydraulic parts, frame, gears, bushings, piston rings, cams, crankshaft, cylinder block, cylinder head, etc.
- Class 200 and class 250 Grey Iron: Can be used in producing gear, cylinder, base, bed, flywheel, cylinder liners, cylinder block, pistons, brake wheel, gear boxes, pressure valve, coupling plate, etc.
- Class 100 and class 150 Grey Iron: Suitable for producing cover body, protective cover, frame, hand wheels, hammer, floor, handle, box, frame, bed, bearing, pulleys, bench, pump body, pipe, valve, etc

Stainless steel 202

Stainless steel 202 is iron carbon alloy having Cr-Ni-Mn composition. The percentage of chromium is more than nickel. Its application includes manufacturing of restaurant equipments, cooking utensils, railways cars and pipelines.

3.2 BOTTOM ASH

Bottom ash was used as an erodent material. It is generated when coal combustion takes place in thermal power plants being heavier in density it does not rise and stay at bottom of the plant. The major constituents of bottom ash are SiO_2 and Al_2O_3.. The Scanning Electron Microscope (SEM) uses the concentrated beam of electrons to generate a range of signals at the surface of the specimen. The electron-sample interaction reveals the morphology of specimen, chemical composition and crystal orientations. The image generated by SEM is high in resolution with greater accuracies. The SEM images were generated at SAI LABS, Thapar University, Patiala (India) using JEOL, 6510LV. The images of bottom ash shows that the size of it approaches nearly as of sand particles and mainly consist of scoriaceous material in which vesicles are empty. The morphology of bottom ash was observed to be angular and irregular with gritty surface textures. Energy Dispersive X-ray spectroscopy (EDS) can be coupled with Scanning Electron Microscope (SEM) to analyse the elemental composition of the specimen as small as few nanometers. The focused beam of electron impacting the specimen produces X-rays which determine the charactertics of the elements present on the specimen. Each elements produce unique sets of X-rays peaks due to different atomic structure. The accuracy of EDS is affected by the escape of X-rays from the sample and also due to overlapping peaks on spectrum. The percentage of SiO_2, Al_2O_3 and CO_2 are 60%, 18% and 20% respectively. The Scanning Electron Microscope and Energy Dispersive Spectroscopy of bottom ash is shown in Figure 3.1.

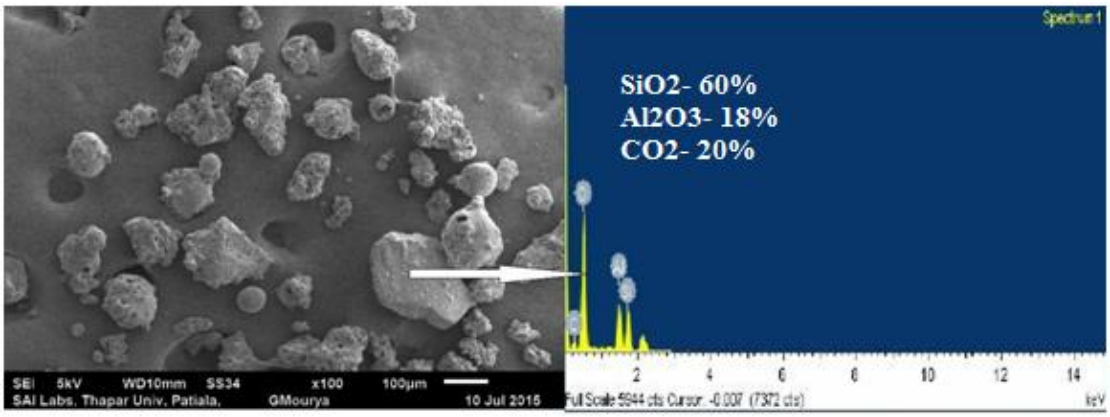

Figure: 3.1 Scanning electron microscope and Energy-dispersive spectroscopy of bottom ash

3.3 CHEMICAL COMPOSITION OF MATERIAL USED

The spectrometer analysis was used to find the chemical composition of Mild steel, Grey cast iron and SS202. The light intensity generated by the arc is used to find the chemical composition of the sample. A spectrometer is used in spectroscopy for producing spectral lines and measuring their wavelengths and intensities. The chemical composition is shown in Table 3.1.

Table 3.1 Chemical composition of Mild steel, Grey cast iron and SS202

Components	Percentage Composition (by Weight)		
	Mild steel	Grey cast iron	SS202
Fe	98.90	55.70	74.50
Cr	0.03	0.11	13.49
Ni	0.03	0.16	0.18
Mn	0.42	1.47	9.64
C	0.13	2.46	0.10
Si	0.16	7.00	0.40
Co	0.01	0.06	0.03
P	0.07	0.80	0.06
Al	0.01	5.75	0.04
Cu	0.06	0.68	1.45
S	0.05	0.15	0.04

3.4 MICRO HARDNESS

Micro hardness of the coated specimen was measured using Vickers diamond pyramid test. The variation in hardness value might be due to different phases on the surface as well as due to anisotropic behaviour of the sample. The distance between the two indentations marks is 50μm. Two or three readings are taken for each of the material and average value is taken as the hardness of material. The hardness value of uncoated material and coated material is shown in Table 3.2 and Table 3.3. After coating it has been observed that micro hardness is considerably increased.

Table 3.2 Hardness value of uncoated base material

Hardness value (Hv)	Mild steel(1015)		Grey Cast iron		SS202	
1	102	106	134	115	181	184
2	098	103	125	127	178	172

Table 3.3 Hardness value of coated base material

Hardness value (Hv)	Mild steel(1015)		Grey Cast iron		SS202	
1	1134	1250	1180	1290	1398	1378
2	1148	1239	1230	1235	1298	1332

3.5 COATING POWDER

Al_2O_3+ 13% TiO_2 (Metco130) is used as a feedstock material for coating purpose with size varying from 10+45μm. The melting point of TiO_2 is low which helps in binding with Al_2O_3 for higher density and better erosion resistance. The erosion resistance of Al_2O_3+ 13% TiO_2 was found to be better than Al_2O_3+ 3% TiO_2 and Al_2O_3+ 40% TiO_2. The coating powder morphology was analyzed using scanning electron microscope. To verify the presence of various elements in coating Energy-dispersive spectroscopy was done. The SEM image showed that morphology of coating powder was fused and crushed with mixed ellipsoid and angular particle shape. The SEM/EDS are shown in Figure 3.2. The percentage elemental composition is 51% Aluminum, 2% Titanium and 46 % Oxygen by weight.

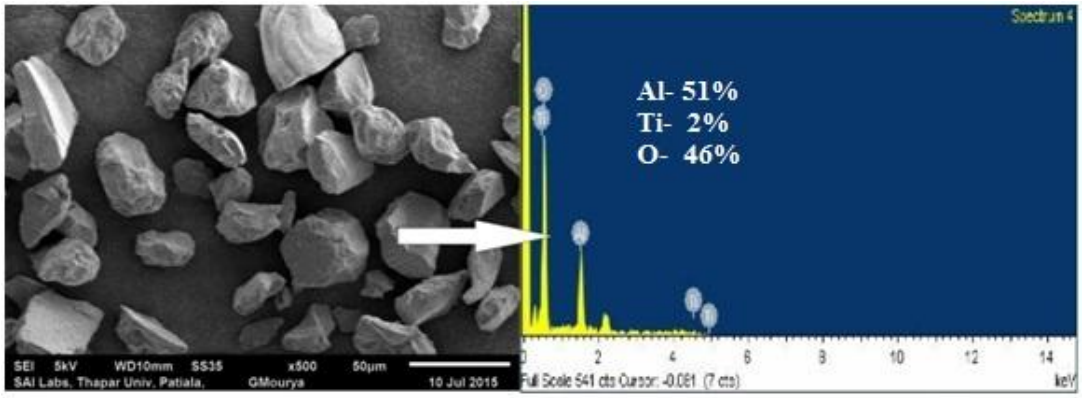

Figure: 3.2 Scanning electron microscope and Energy-dispersive spectroscopy of powder

3.6 COATING DEPOSITION

In industries due to severe environmental conditions there is always premature loss of material from the component surface. The surface requirement of the component varies with the service conditions. But in actual practical conditions there is more than one service condition acting on the component like abrasive wear with thermal stress.

3.6.1 Thermal Spray Coating

Thermal spraying process is defined as applying of coating in which molten particles are propelled at high speed on the surface of the substrate.

It is further classified into four different categories.

- **Flame powder spray** the powder feedstock is melted in the gaseous flame and deposited on the base material. The advantage is larger number of coating powder can be melted and propelled at high speed on the surface. The heat source is due to the reaction between fuel and oxygen.
- **Electric arc wire spray** with electric arc wire spray, an arc is formed by contact of two oppositely charged metallic wires, usually of the same composition. This leads to melting at the tip of the wire material. The rate of spray is adjusted by regulation of wire feed.
- **Plasma spraying process** a high frequency arc is ignited between tungsten cathode and anode. Three different gas (Helium, Hydrogen and nitrogen) are used to generate plasma between the electrodes. The temperature at the centre can reach about 16000 K. The spray powder is feed into the plasma flume which is propelled to get deposit on the substrate.
- **High velocity oxy-fuel** Molten or semi-molten materials are sprayed onto the surface by means of the high temperature, high velocity gas stream, producing a dense spray coating which can be ground to a very high surface finish. Comparison is shown in Table 3.4.

Table 3.4 Comparison of different Thermal Spray coating

Charactertics	Powder flame spray	Electric arc spray	Plasma spray	High velocity Oxy-fuel
Gas temperature (^{0}C)	3000^0 C	4000^0 C	12000-16000^0 C	2600^0 C
Spray rate (kg/h)	2-6	10-25	2-10	1-9
Particle velocity (m/sec)	50	150 approx	Up to 450	700
Hardness (HRC)	35-55	35-40	40-65	45-60
Porosity (%)	3-15	4-5	Less than 2	2-4

Prior to coating deposition the specimen was grit blasted with abrasive particles for proper absorption. For specialized applications, a variation of the process is to plasma spray in a controlled, low pressure atmosphere. In contrast to coating in air (atmospheric plasma spraying, or APS), the melted particles oxidize far less with vacuum plasma spraying (VPS), resulting in coatings of considerably higher quality The plasma spraying was deposited at M/S Metalizing Equipment Company private Limited, Jodhpur (India). The operating parameters for coating deposition are given in Table 3.5. The coating thickness of 100μm was deposited.

Table 3.5 Operating parameters of Atmospheric Plasma Spraying (APS)

Primary gas flow rate (Argon)	70-80 lpm
Carrier gas flow rate (Nitrogen)	33-40 lpm
Secondary gas flow rate (hydrogen)	17-20 lpm
Powder feed	40-45 grams/min
Spray distance	100 mm
Current	500 Ampere
Voltage	60-70 Volts

CHAPTER 4 EXPERIMENTION AND RESULTS

4.1 SLURRY POT TESTER

The erosion resistance of the given sample is evaluated using slurry pot tester TR 41 (Ducom, India). The test data will rank the materials according to their mass loss and also helps to study the effect of coating material on the mass loss of the given sample. Test rig consists of frame, spindle, stirrer and control system. The main component is fixed inside the frame and the frame is made of rigid material to avoid vibration. The slurry cup is dipped into water jacket and the jacket is moved up and down using screw jack given at the bottom of the tester. The spindle rotation is controlled by ac motor with variable frequency drive. The sample to be tested is placed between the spindle and the stirrer. The capacity of slurry cup was around 1.2 liters. The various components is shown in Figure 4.1

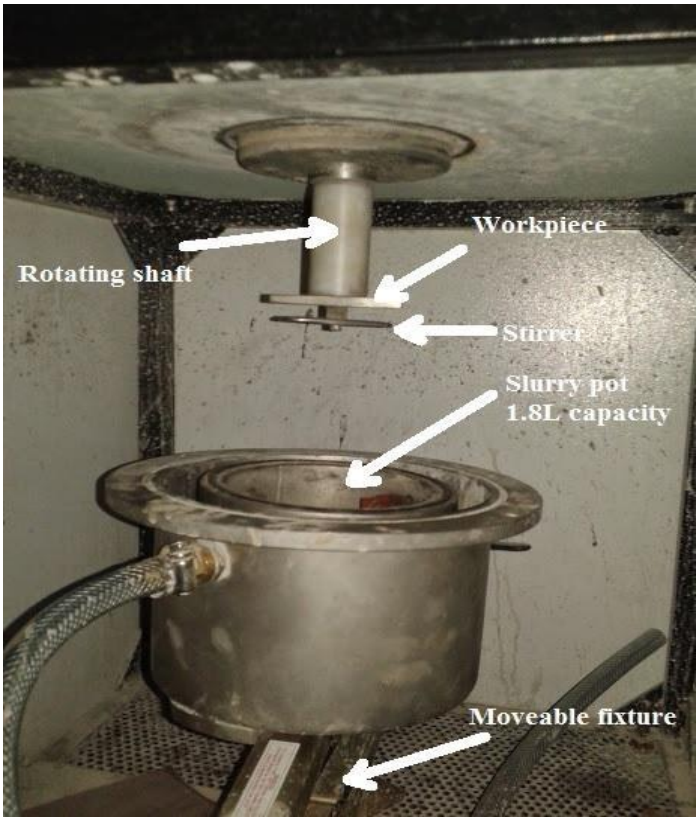

Figure: 4.1 DUCOM slurry pot tester

4.2 PREPARATION OF SLURRY

To prepare slurry the pot is first cleaned thoroughly and the measured weight of erodent particle mixed with water is poured into the pot and then it's properly stirred till uniform mixture is formed. The sample is weight using weighing machine with least count of 0.0001 mg. To prepare 50 % concentration 300 grams of bottom ash is mixed with 300 grams of water.

Figure: 4.2 Slurry Pot

4.3 SPECIMEN

Typical specimen is rectangular shape 25.4 X 76mm X 6.35 thickness. The specimen were cut using power hack saw from large sheet of given materials. The schematic diagram of the specimen is shown in Figure 4.3.

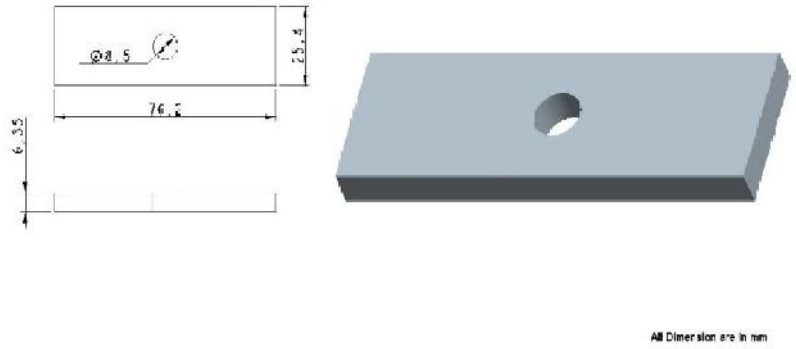

Figure: 4.3 Dimensions of specimen used

4.4 EXPERIMENTAL PARAMETERS

Erosion of all the three materials Mild steel, SS 202 and grey cast iron without and with coating is tested on slurry pot tester by using bottom ash as erodent material at different test conditions as given in Table 4.1.

Table 4.1 Experimental parameters and specification

Parameters	**Specifications**
Material	Mild steel, SS 202 and grey cast iron
Erodent material	Bottom ash
Particle size (μm)	75-150μm 150-250μm and 250-350μm
Slurry concentration (C_w)	25 and 50
Speed (RPM)	700 ,1000 and 1400
Time (min)	90 and 180

4.5 EFFECT OF ROTATIONAL SPEED ON THE EROSION RATE

Erosion rate is a function of kinetic energy of the impacting particles, as we know that increasing rotational speed increases the velocity of impact, so it is quite expected that erosion rate will increase. In the present work, the relative velocity of the work piece and the impacting particles is proportional to the rotational speed of the spindle carrying the work piece. Value of exponent α for Mild steel , grey cast iron and SS 202 based upon experimental results was found to be 1.96 , 1.73 and 1.53 which in good agreement with (Goyal et.al 2012) it is concluded effect of velocity is more in Mild steel as compared to SS202 and grey cast iron. The value of exponent α lies in the range of 1 to 1.35. The effect of velocity is maximum in case of mild steel and minimum in case of SS202.

Figure 4.4 shows mass loss of 25 % concentration at 90 min. From the figure it shows that percentage increase in mass loss during early cycles is more as compared to latter cycles. Wear of mild steel is found more than other two materials, it is certainly due to the less micro hardness of mild steel as compared to other two materials. It has been also observed that percentage increase in mass loss of mild steel from 700 rpm to 1000 rpm is more as compared to grey cast iron, but during later cycles from 1000 to 1400 grey cast iron showed more percentage of mass loss as compared to mild steel. The reason behind for showing this type of trend is due to brittle nature of grey cast iron. From the Figure it has been observed that erosion resistance of coated SS202 is best among the others due to very high micro hardness. The reason behind for more mass loss during early cycles is due to fresh abrasive slurry impacting on the surface of sample but as the sharp edges of abrasive gets destroyed it lead to less erosion loss.

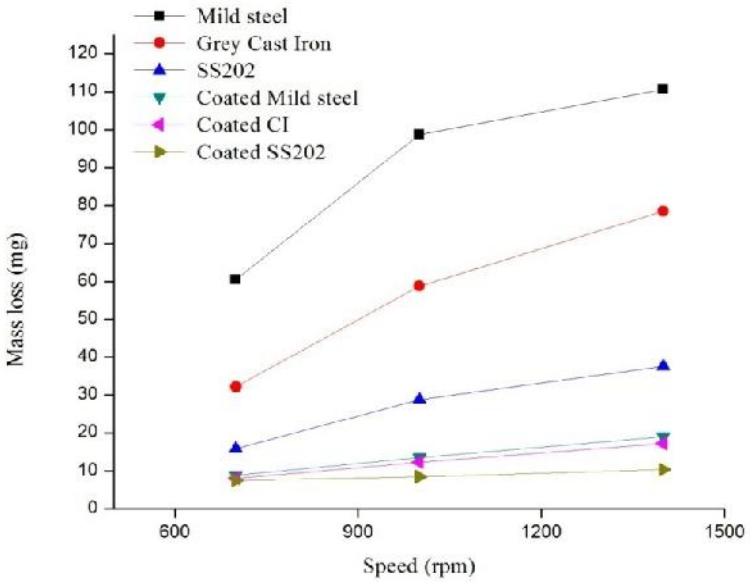

Figure: 4.4 Weight loss (Cw=25 %) at 90 min

At 50 % concentration with 90 min the trend shown by the materials somewhat gets changed due effect of concentration on erosion rate of the sample. The percentage mass loss at higher speed was found to be more than 25 % concentration at similar time due to presence of more number of sharp abrasive, with increase in speed the kinetic energy for striking the surface increase. The combined effect of speed and concentration shows that there might be some interaction between speed and concentration. Figure 4.5 shows mass loss of 25 % concentration at 180 min.

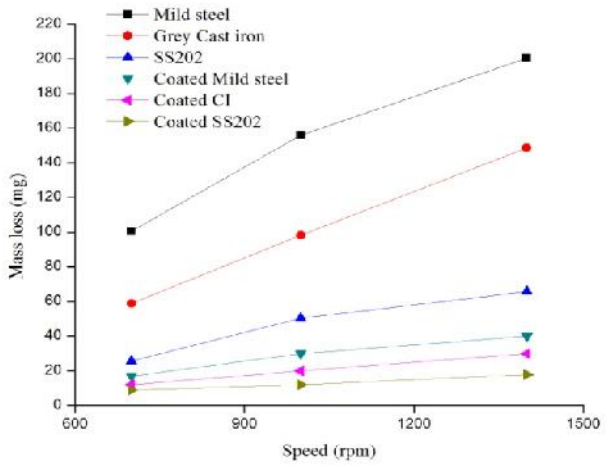

Figure: 4.5 Weight loss (Cw=25 %) at 180 min

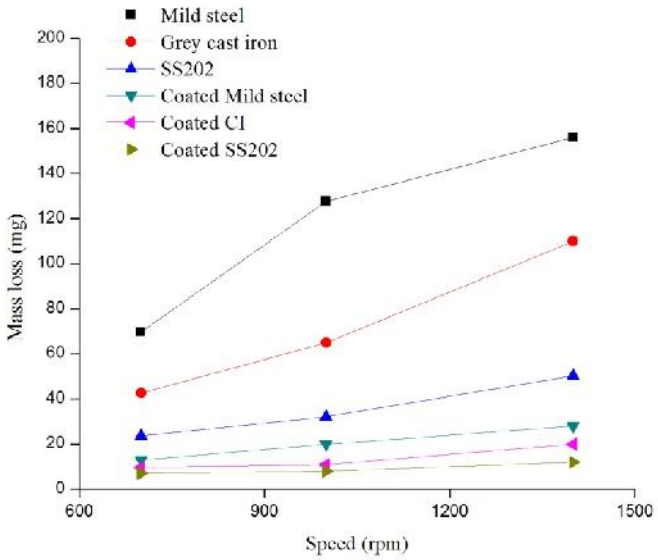

Figure: 4.6 Weight loss (Cw=50 %) at 90 min

Erodent particle speed have a great influence on the wear of piping materials, as it is clear from Figure. 4.6 for the 90 min tester run with 50 % concentration. But at greater speeds wear is found to be decreased and that may be due to because at higher speeds erodent particle motion is so random that inter particle collisions are more and these collisions are causing decrease in the momentum of erodent particles, which may lead to decrease in mass loss at higher speeds

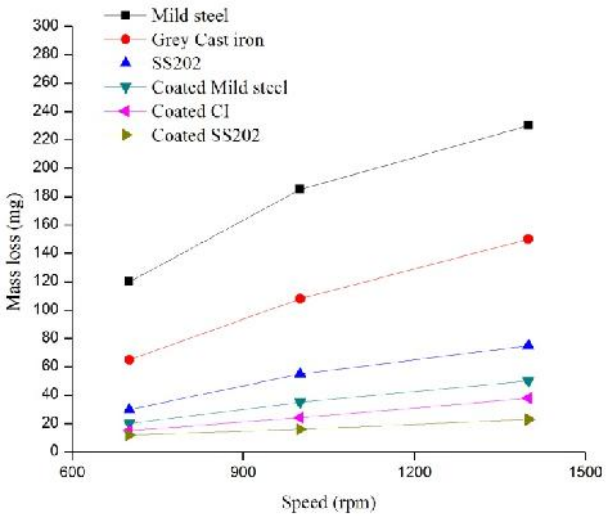

Figure: 4.7 Weight loss (Cw=50 %) at 180 min

4.6 EFFECT OF CONCENTRATION OF BOTTOM ASH ON EROSION RATE

The effect of slurry concentration is shown in figure, from the given figure we observed that as the slurry concentration increase, erosion rate also increases. Value of exponent γ for the Mild steel, grey cast iron and SS 202 on the basis of experimental study was found to be 0.49, 0.5 and 0.36 respectively. The value of coated sample is 0.33 0.4 and 0.25 for mild steel, grey cast iron and SS202. This value of exponent is in correlation with values obtained by the previous researchers (Goyal.et al 2012). The value of exponent γ is found to be less than 1, this might be due to lesser number of particles impacting the target surface, while most of the particles did not strike and lost their way while colliding with other particles. These limits are showing same as found by Gupta et al. (1995), Goyal et al. (2012) and Goyal et al. (2014), expected value of exponent γ is expected to be below 1 as proposed by researchers.

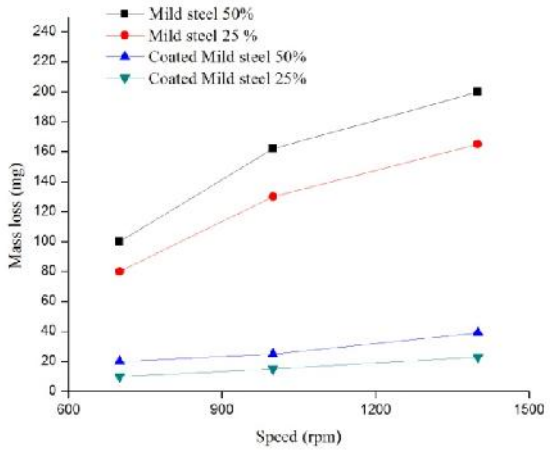

Figure: 4.8 Relative erosion of mild steel at 90 min

It is clear from above figure. That more is the concentration more is the wear of testing material, again at large concentrations inter particle motion gets so disturbed that average momentum of erodent particles gets decreased and number of particles striking per unit time with testing material gets decreased, which may lead to decrease in the mass loss at together at higher concentration and higher speeds.

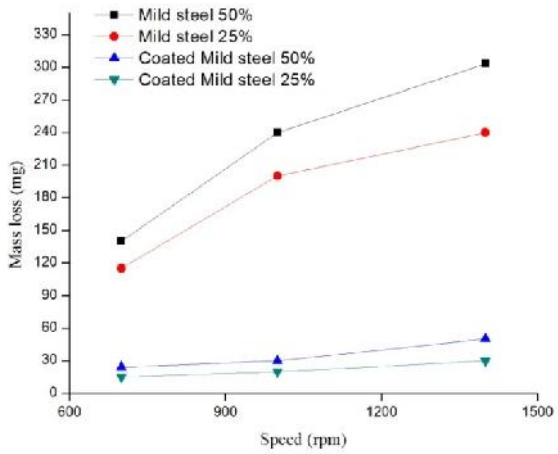

Figure: 4.9 Relative erosion of mild steel at 180 min

From the above figure it has been observed that if time is doubled, the erosion rate due concentration is not doubled due to non-linear relation between these, it may be due to dull out of new erodent particles at earlier stages of experiment and also due to metallurgical changes in the properties of testing materials because as long as test proceeds, temperature of the slurry gets increases, consequently there are effects on the erosion phenomenon.

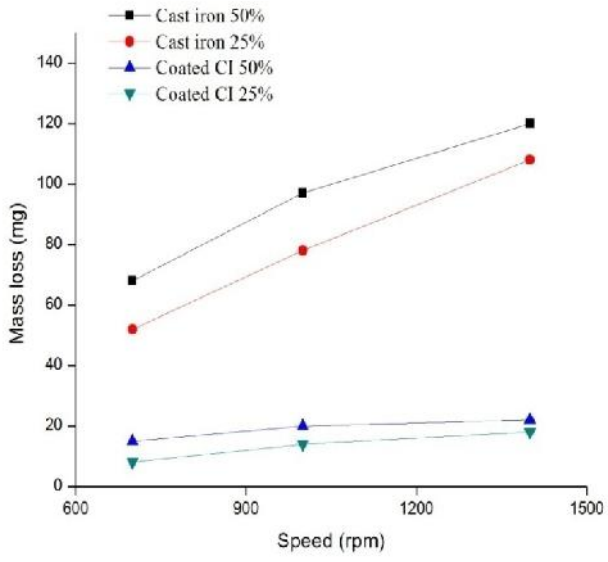

Figure: 4.10 Relative erosion of grey cast iron at 90 min

The figure above shows the mass loss of Grey cast iron at different concentration.

The mass loss is different from mild steel under similar erosion conditions due to different microstructure present and also due to dissimilar erosion mechanism. The erosion resistance was improved in all three materials due to higher hardness of coating substrate.

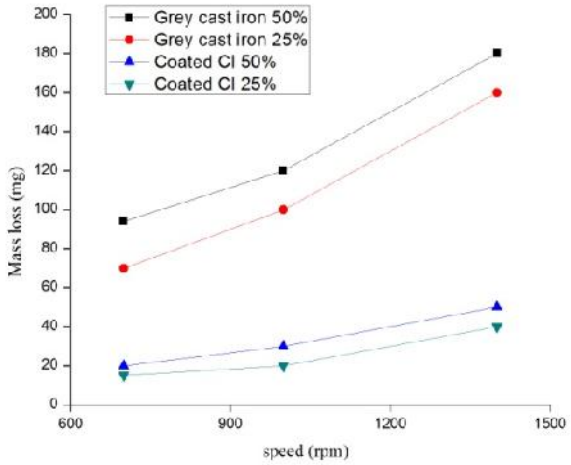

Figure: 4.11 Relative erosion of grey cast iron at 180 min

4.7 EFFECT OF PARTICLE SIZE ON EROSION RATE

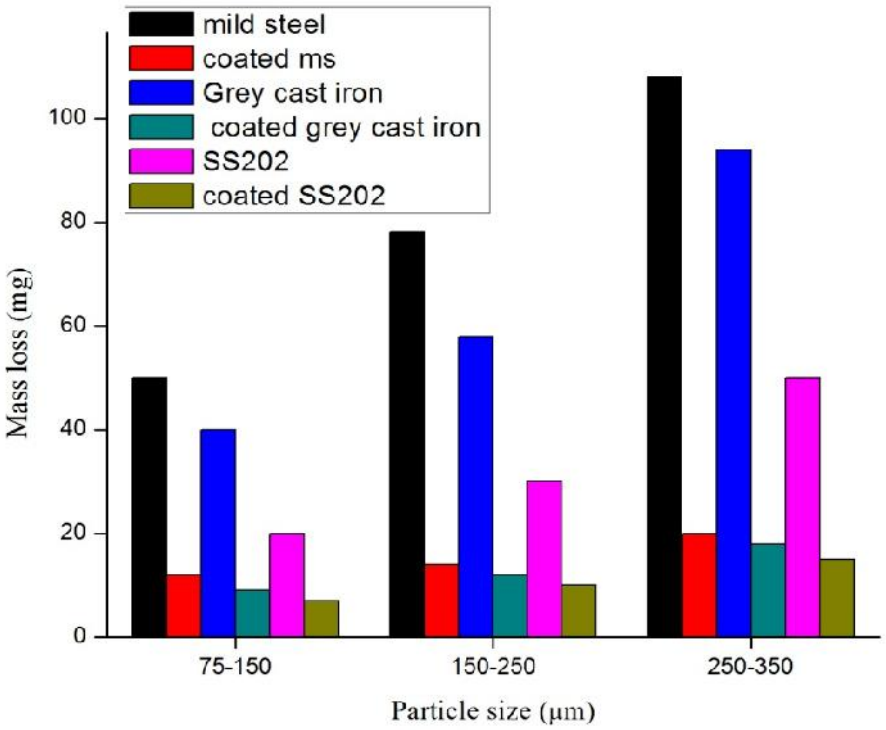

Figure: 4.12 Particle size on erosion rate

The effect of particle size on erosion rate is shown in above figure. As particle size increase the erosion rate of mild steel increase considerably. From the results it is seen that the erosion rates increase with increase in average particle size. This increase in the erosion rate with increase in average particle size is mainly due to the increase in kinetic energy of impacting particles.

4.7 EROSION MECHANISM

To study the erosion mechanism of uncoated and coated specimen, Scanning electron microscope images were taken at 90 min and 180 min uncoated mild steel. The effect of particle size on erosion mechanism is observed using two different SEM image with two different particle sizes on coated mild steel. SEM image taken for eroded specimen were for 50 % concentration of bottom ash and 1400 rpm.

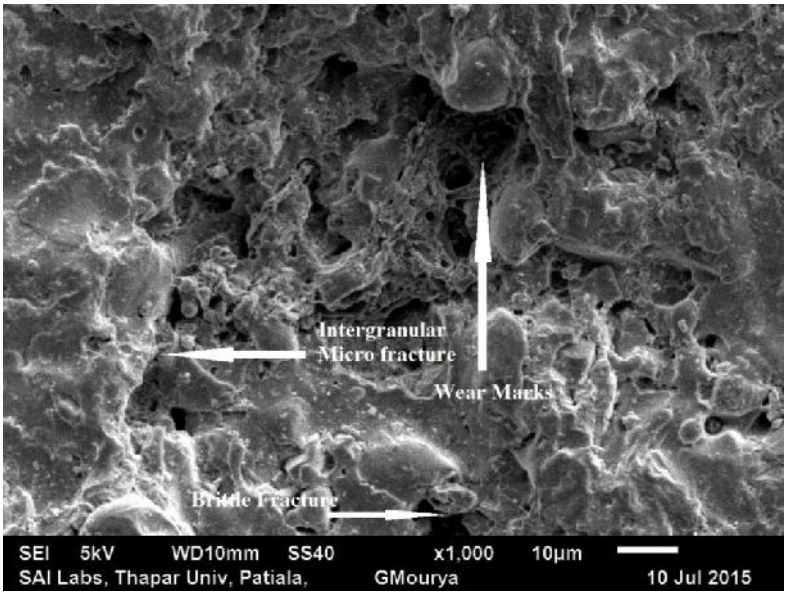

Figure: 4.13 SEM micrograph of coated mild steel with erodent size 250-350«m

The SEM morphology of eroded mild steel with coating showed the presence of grooves, wear marks, brittle fracture and inter granular micro fracture when subjected to erodent particle size between 250-350 μm is shown in above figure. The cracks developed due to high thermal stress encountered during atmospheric plasma spraying.

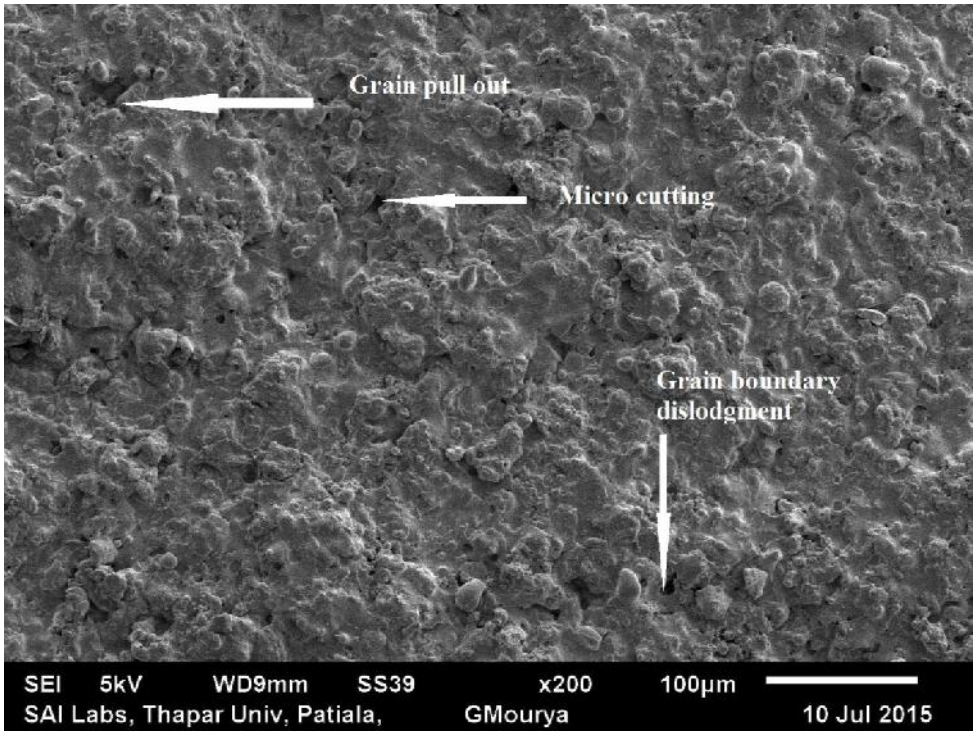

Figure: 4.14 SEM micrograph of coated mild steel with erodent size 75«m

The above SEM micrograph shows that when particle size decreases to 75 µm the erosion mechanism changes its nature from brittle fracture to grain dislodgment. The grain dislodgment is due to the presence of un melted particles on the surface of Al_2O_3 + 13% TiO_2 coated sample. It also observed that when particle size is reduce the erosion resistance of coated sample increase due to less critical energy supplied erodent particle. Critical energy in erosion is defined as the minimum or threshold energy required to pull out material from the surface of the specimen or substrate.

SEM micrographs show that the erosion mechanism is due to single or multiple splat removal through crack propagation along the boundaries.

The uncoated mild steel was observed for 90 min and 180 min. The SEM micrographs at 90 min and 180 min showed that mild steel display plastic deformation at 90 min with small craters while at 180 min the nature of erosion mechanism remains same with large sized craters, some multiple ploughing and plastic deformation. The shape of wear scars did not changed with time except that they got bigger due to continuous impingement of abrasive erodent for longer time. The shape of scar is appears to be irregular while some has spherical shape.

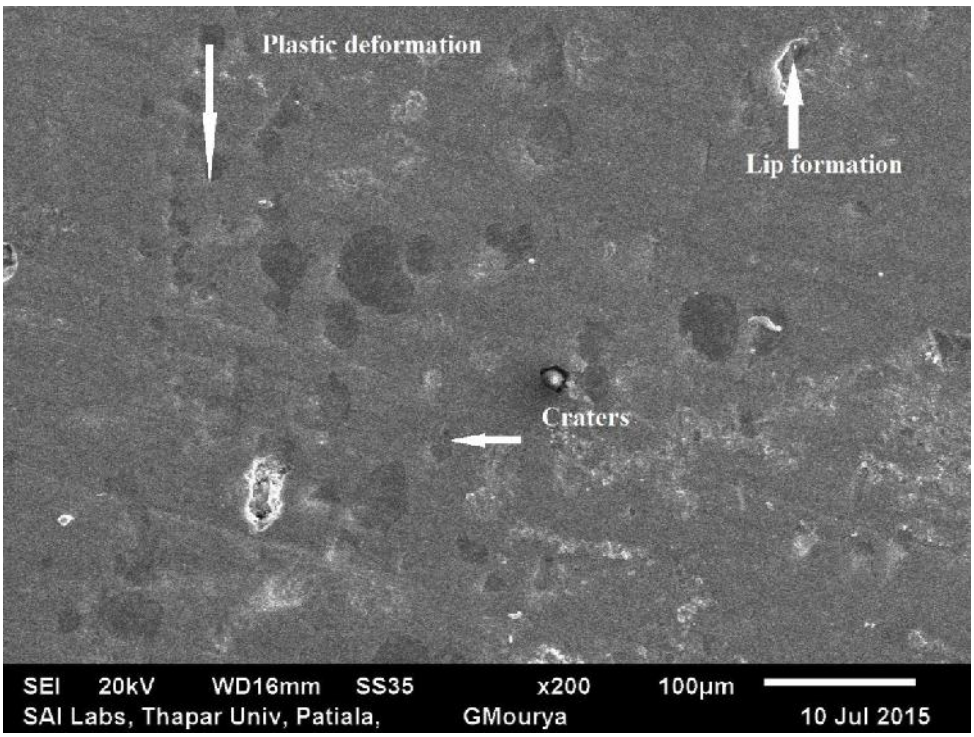

Figure: 4.15 SEM micrograph of mild steel at 90 min

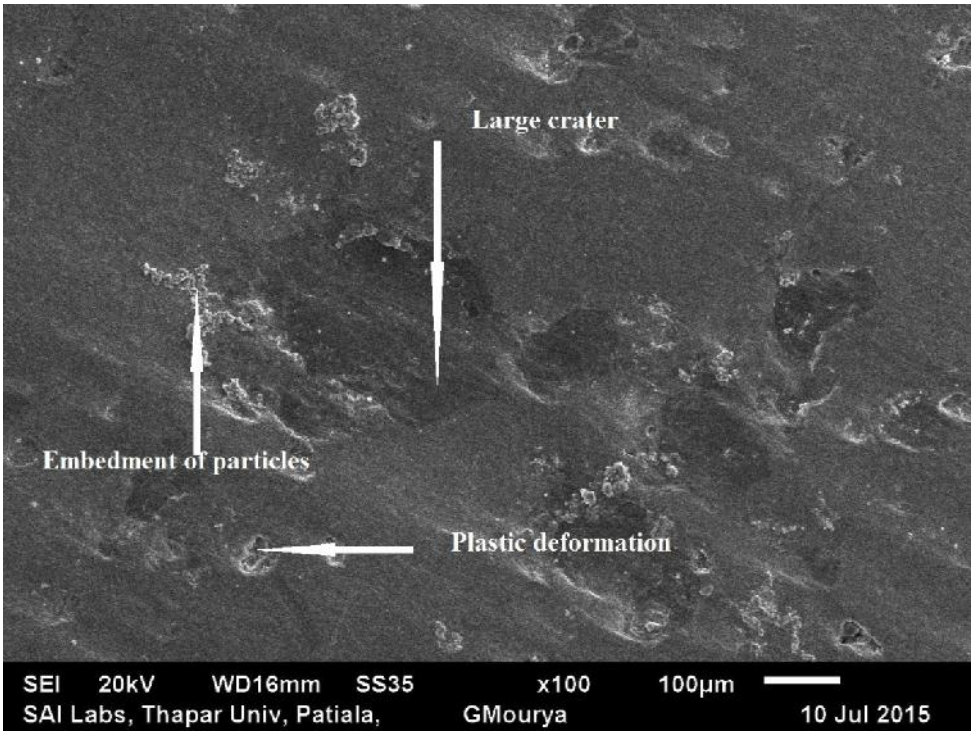

Figure: 4. 16 SEM micrograph of mild steel at 180 min

The erosion mechanism shown by Al_2O_3 + 13% TiO_2 coated sample is combination of grain boundary dislodgment due to fracture and lateral crack chipping. Crack usually propagated through grain boundary due to lesser energy needed that the crystalline cleavage. Major cause of micro fracture in Alumina titania coating is due dislocation pile up against grain boundaries that in turn triggers grain pull out.

CHAPTER5 OPTIMIZATION OF PARAMETERS USING FUZZY LOGIC AND NEURAL NETWORKS

5.1 INTRODUCTION

Fuzzy logic is one of the artificial intelligence techniques that have ability to tackle the problem of complex relationships among variables that cannot be accomplished by more traditional methods.It is a mathematical theory of inexact reasoning that allows modeling in linguistic terms of the reasoning process of human. It is widely used for engineering, medical, economical problems and particular applications in very complex industrial systems. Fuzzy controllers and fuzzy reasoning are suitable in defining the relationship between system inputs and desired outputs. The theory on fuzzy set admits the existence of a type of uncertainty (or indecision) in process decision variables due to vagueness (referred to as 'fuzzy uncertainty') rather than due to randomness alone, and many decisions in process control are in fuzzy environment .Fuzzy set theory-based modeling technique is generally preferred when subjective knowledge or opinion(s) of process expert(s) play a key role in defining objective function and decision variables. Shin & Vishnupad (1996) observe that the fuzzy and ANN-based modeling techniques are an effective means of control in complex grinding process. Kou & Cohen (1998) emphasize the importance of integration between fuzzy and ANN-based technique for effective process control in manufacturing. The degree of membership function of an object in a fuzzy set is defined by membership functions which help in determining fuzzy values.Thus optimization of the process has eluded industry for over five decade due to inadequate understanding of material process interaction and process fundamentals. In fuzzy logic most widely used shape for membership function are; triangular, Gaussian, trapezoidal and arcs. Many researchers suggest different kind of membership function like (Babuska, 1998) found out that trapezoidal and triangle membership shapes is better of rock cutting trencher. The data used for optimizing parameters is taken from the open literature [16].The Mamdani implication method is employed for fuzzy inference reasoning in this paper. The triangular shape membership function has been selected for optimizing the process variable selected for slurry erosion behavior.

5.2 PRINCIPLES OF FUZZY LOGIC

Modeling of fuzzy logic is employed using rule based system. In rule based the variables used in fuzzy system is based on if- then rules:

IF (x_1 is A_1, x_2 is A_2…….x_n is A_n) THEN (y_1 is B_1, y_2 is B_2,……y_n is B_n)

Where linguistic variables x_1, y_1 take values of fuzzy sets A_1 and B_1 respectively. The rule based is shown in appendix. The schematic diagram of structure of fuzzy system is shown in Figure 5.2.

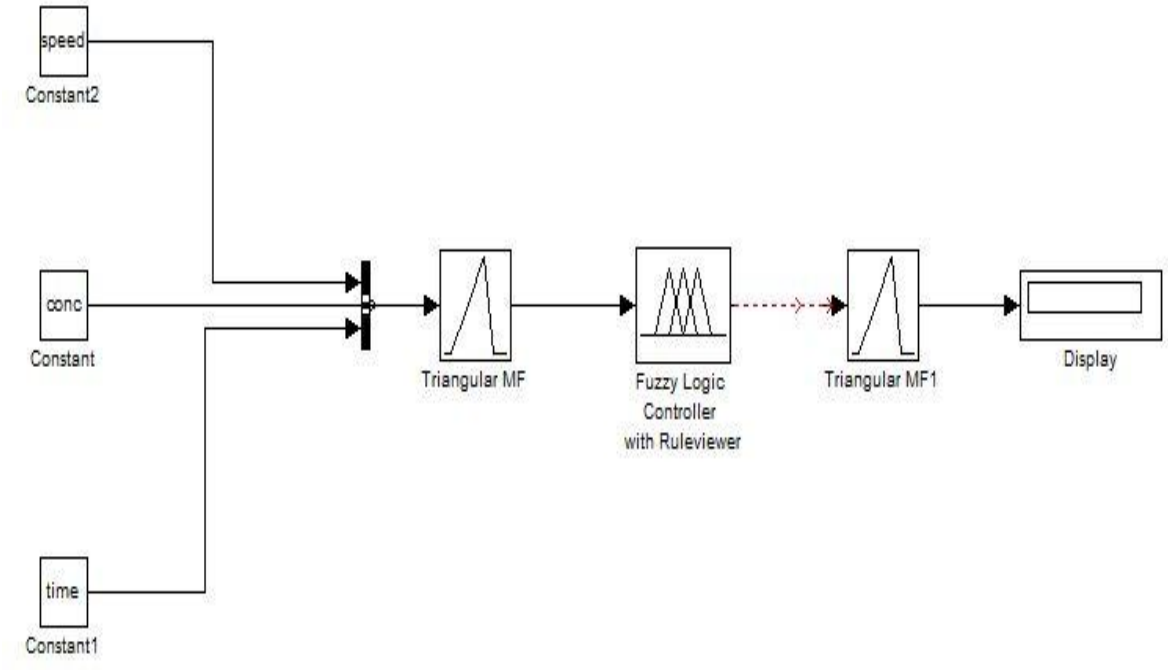

Figure: 5.1 Structure of fuzzy system

There are five different defuzzification methods: centroid, bisector, middle of maximum, largest of maximum, and smallest of the maximum. The most popular method is Centroid (Yamaguchi, 1991). The membership function for speed, concentration and time is defined:

$$\text{Triangle (X a, b, c)} \begin{cases} 0 & x \leq 800 \\ \frac{X-a}{b-a} & 800 \leq x \leq 1100 \\ \frac{c-X}{c-b} & 1100 \leq x \leq 1400 \\ 0 & 1400 \leq x \end{cases} \quad (5.1)$$

The mamdani FIS is implemented in MATLAB 7.10. The input and output member ship function is shown Figure 5.2

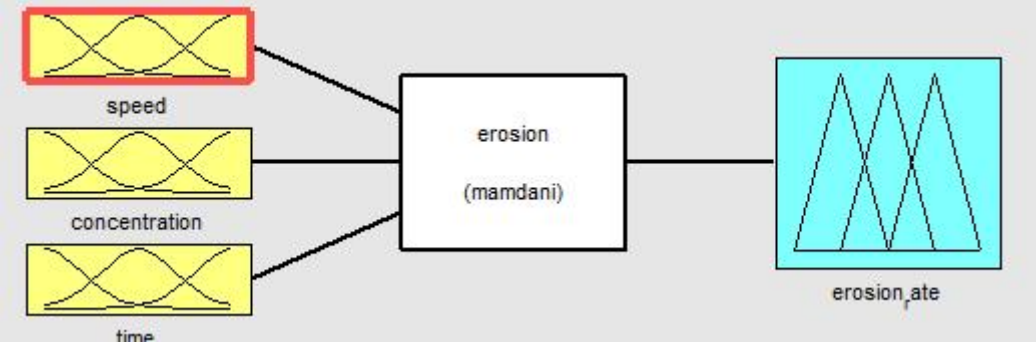

Figure: 5.2 Mamdani Fuzzy Interference System

5.3 ALGORITHMS USED IN FUZZY LOGIC

There are five steps in fuzzy logic:

- Step number one is related to defining of linguistic variable and terms which is termed as initialization. In linguistic variable the input and output are termed in words rather than in numerical values. For example in our study we defined speed as low, low medium, medium and high.
- Second step is related to membership function. Membership function is used in fuzzification and defuzzification to convert the non fuzzy values into linguistic terms and vice versa.
- Fuzzy rules are used in FIS to control the output variable.
- Fuzzy set operation is fourth step. The evaluations of the fuzzy rules and the combination of the results of the individual rules are performed using fuzzy set operations. The operations on fuzzy sets are different than the operations on non-fuzzy sets. Let μ_A and μ_B are the membership functions for fuzzy sets A and B operations for OR and AND operators on these sets, comparatively. The mostly- used operations for OR and AND operators are max and min respectively. For complement (NOT) operation, Eq is used for fuzzy sets

$$\ll \underset{A}{\rightarrow} (x) = 1 \qquad \mu_A (x) \ldots\ldots\ldots \tag{5.2}$$

Table 5.1 Fuzzy rules

Fuzzy rules
1 IF (speed is low) AND (concentration is low) AND (time is low) THEN erosion rate is lowest
2 IF (speed is high) AND (concentration is high) AND (time is high) THEN erosion rate is highest

- Defuzzification is fifth and final step in fuzzy logic. After interference the output values are defuzzfied into crisp values. Defuzzification is performed according to membership function of the output variable. The different defuzzification algorithms are shown in Table 5.2.

Table 5.2 Defuzzification Algorithms [4]

Operations	Formula
Centre of gravity	$\frac{\int_{min}^{max} u\,\mu(u)\,du}{\int_{min}^{max} \mu(u)\,du}$
Left most max	$U - in\,f(u)$
Right most max	$U - sup\,(u)$

The experimental data with fuzzy prediction is shown below in Table 5.3, 5.4 and 5.5

Table 5.3 Experimental and fuzzy prediction for uncoated mild steel

Exp no	Speed	Concentration	time	Mass loss M.S (mg)	Fuzzy	%error
1	500	25	90	39.6	39.6	0.25
2	500	25	180	72.9	63.9	12.34
3	500	45	90	52.4	40.6	22.51
4	500	45	180	99.8	94.3	5.51
5	800	25	90	64.3	63.9	0.62
6	800	25	180	124.1	125	0.72
7	800	45	90	111.8	109	2.50
8	800	45	180	211.9	195	7.97
9	1100	25	90	95.9	94.3	1.66
10	1100	25	180	184.5	195	5.69
11	1100	45	90	151.8	124	18.31
12	1100	45	180	193.8	194	0.25
13	1400	25	90	111.7	108	2.86
14	1400	25	180	217.8	219	0.55
15	1400	45	90	182.7	218	19.32
16	1400	45	180	343.5	260	24.30

The 3-d plots show the variation of erosion rate with speed, concentration and time. It shows that the effect of concentration is minimum on erosion rate while the most significant factor for erosion is speed.

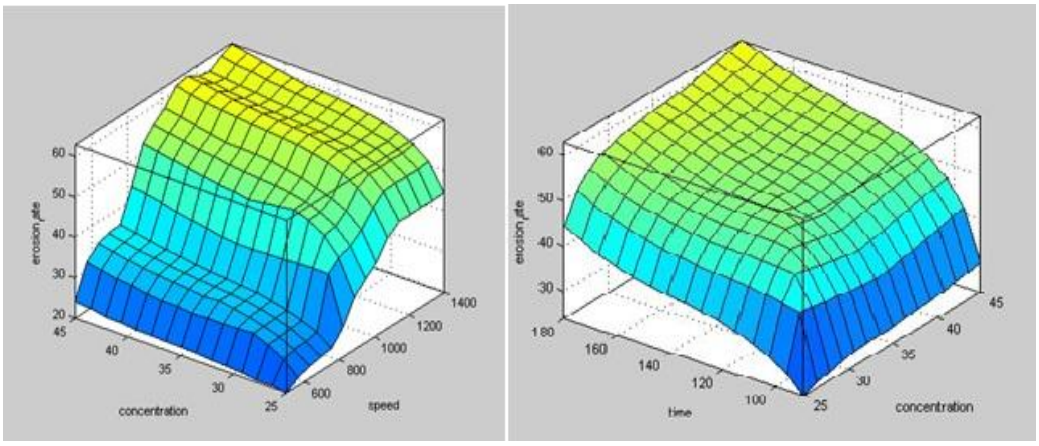

Figure: 5.3 3-D Surface Plot for erosion rate with speed concentration and time for mild steel

Table 5.4 Experimental and fuzzy prediction for coated mild steel

Exp no	Speed	Cw %	Time	Coated Mild steel(mg)	Fuzzy	% error	Coated Ni M.S	Fuzzy	% error
1	500	25	90	8.60	8.68	0.93	15.9	16.0	0.62
2	500	25	180	9.10	8.78	3.51	20.5	20.4	0.48
3	500	45	90	11.20	10.50	6.25	16.2	15.9	1.85
4	500	45	180	16.90	16.40	2.95	26.8	25.2	5.97
5	800	25	90	11.80	10.60	10.16	24.7	20.5	17.00
6	800	25	180	15.80	14.40	8.86	32.5	29.5	9.23
7	800	45	90	16.70	16.50	1.19	28.3	25.2	10.95
8	800	45	180	30.20	29.00	3.97	47.9	42.5	11.27
9	1100	25	90	15.60	14.50	7.05	29.5	29.6	0.33
10	1100	25	180	24.90	24.40	2.00	52.9	52.5	0.75
11	1100	45	90	21.60	19.20	11.11	40.1	34.0	15.21
12	1100	45	180	38.30	37.40	2.34	74.4	72.1	3.09
13	1400	25	90	19.10	19.20	1.04	32.3	29.8	7.73
14	1400	25	180	29.70	29.00	2.35	57.4	52.5	8.53
15	1400	45	90	26.60	24.50	7.89	47.2	42.5	9.95
16	1400	45	180	43.10	37.00	14.15	89.1	72.1	19.07

Table 5.5 Experimental and fuzzy prediction for uncoated SS202

Exp no	Speed	Concentration	time	Mass loss SS202	Fuzzy	%error
1	500	25	90	14.3	15.9	11.18
2	500	25	180	23.8	21.0	11.76
3	500	45	90	19.8	15.8	20.20
4	500	45	180	34.8	34.0	2.29
5	800	25	90	24.7	21.0	14.97
6	800	25	180	42.2	39.1	7.34
7	800	45	90	31.1	29.8	4.18
8	800	45	180	58.1	50.5	13.08
9	1100	25	90	31.9	29.8	6.58
10	1100	25	180	59.3	60.4	1.85
11	1100	45	90	40.2	39.1	2.73
12	1100	45	180	75.4	77.9	3.31
13	1400	25	90	36.2	34.0	6.07
14	1400	25	180	68.6	60.6	11.66
15	1400	45	90	53.2	50.1	5.82
16	1400	45	180	99.1	78.3	20.98

Table 5.6 Experimental and fuzzy prediction for coated SS202

Exp no	Speed	Concentration	time	Coated SS202(mg)	Fuzzy	%error	Coated Ni SS202	Fuzzy	%error
1	500	25	90	6.3	7.16	13.65	12.2	12.8	4.91
2	500	25	180	9.2	7.20	21.73	15.9	16.5	3.77
3	500	45	90	9.8	8.72	11.02	14.4	12.9	10.4
4	500	45	180	14.8	12.7	14.18	24.5	22.4	8.57
5	800	25	90	10.1	15.6	24.75	19.3	16.6	13.9
6	800	25	180	17.6	15.7	10.79	25.8	25.2	2.32
7	800	45	90	15.7	16.2	3.18	23.4	22.4	4.27
8	800	45	180	27.6	25.6	7.24	42.7	44.0	3.04
9	1100	25	90	13.4	12.8	4.47	24.7	25.4	2.83
10	1100	25	180	21.8	21.3	2.29	40.6	42.3	4.18
11	1100	45	90	19.6	18.2	7.142	31.8	29.1	8.49
12	1100	45	180	35.5	37.40	5.352	62.8	61.4	2.22
13	1400	25	90	19.2	18.30	4.687	29.7	30.0	1.01
14	1400	25	180	27.4	25.7	6.204	48.6	44.0	9.46
15	1400	45	90	22.5	21.4	4.888	38.4	36.9	3.90
16	1400	45	180	43.10	37.00	14.15	89.1	72.1	19.07

From 3- D Surface plot shown in Figure 5.4 the effect of speed is maximum on erosion rate while the effect of time is minimum on erosion rate.

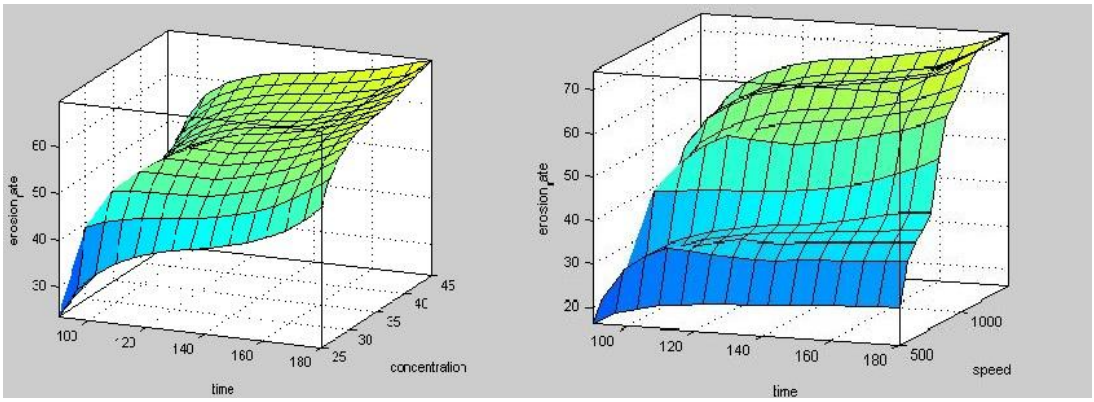

Figure: 5.4 3-D Surface Plot for erosion rate with speed concentration and time for SS202

Table 5.7 Experimental and fuzzy prediction for uncoated SS304

Exp no	Speed	Concentration	time	Mass loss SS304	Fuzzy	%error
1	500	25	90	19.6	21.9	11.73
2	500	25	180	36.6	33.2	9.289
3	500	45	90	27.7	22.3	19.49
4	500	45	180	51.1	45.3	11.35
5	800	25	90	35.4	33.5	5.367
6	800	25	180	63.7	65.1	2.197
7	800	45	90	56.3	55.1	2.131
8	800	45	180	103.8	99.8	3.853
9	1100	25	90	48.4	45.3	6.405
10	1100	25	180	92.4	83.9	9.199
11	1100	45	90	73.7	65.8	10.71
12	1100	45	180	139.1	135	2.731
13	1400	25	90	57.5	55	4.347
14	1400	25	180	103.5	100	3.381
15	1400	45	90	85.2	83.9	1.525
16	1400	45	180	162.6	135	16.97

Table 5.8 Experimental and fuzzy prediction for coated SS304

Exp no	Speed	Concentration	time	Coated SS 304(mg)	Fuzzy	%error	Coated Ni SS 304	Fuzzy	%error
1	500	25	90	5.9	6.2	5.084	13.6	12.8	5.88
2	500	25	180	7.7	7.6	1.298	20.1	19.5	2.98
3	500	45	90	5.2	7.32	21.53	14.8	12.9	12.83
4	500	45	180	8.9	11.3	26.96	27.8	23.6	15.10
5	800	25	90	7.6	7.9	3.947	22.1	24.3	9.95
6	800	25	180	10.2	11.2	9.803	31.5	31.2	0.95
7	800	45	90	9.1	9.3	2.197	24.4	23.6	3.27
8	800	45	180	14.7	14.6	0.680	48.6	48.9	0.61
9	1100	25	90	9.5	10.3	8.421	26.7	22.3	16.47
10	1100	25	180	17.2	18.2	5.814	48.9	46.8	4.29
11	1100	45	90	11.8	13.4	13.55	37.9	38.9	2.63
12	1100	45	180	23.3	24.5	5.150	69.1	65.4	5.35
13	1400	25	90	12.1	13.1	8.264	30.2	30.0	0.66
14	1400	25	180	19.6	19.9	1.530	59.1	52.7	10.82
15	1400	45	90	14.1	14.5	2.836	48.9	48.6	0.61
16	1400	45	180	25.8	22.3	13.56	83.1	72.5	12.75

5.4 ARTIFIICAL NEURAL NETWORKS

5.4.1 Basic concept of neural networks

Neural networks, which are simplified model of the biological neuron system, is a massively parallel distributed processing system made up of highly interconnected neural computing elements that have the ability to learn and thereby acquire knowledge and make it available for use. Hence, the technology, which has been built on a simplified imitation of computing by neurons of a brain, has been termed Artificial Neural System (ANS) or Artificial Neural Network (ANN). In the literature, this technology is also referred to as connectionist network, Neuro-computers, parallel distributed processors etc. Also neurons are referred to as neurodes, processing elements (PEs) and nodes. The behavior of a neuron can be captured by a simple model shown in Figure…. Every components of the model bears a direct analogy to the actual constituents of a biological neuron and hence is termed as artificial neuron. It is this model which forms the basis of Artificial Neural Network.

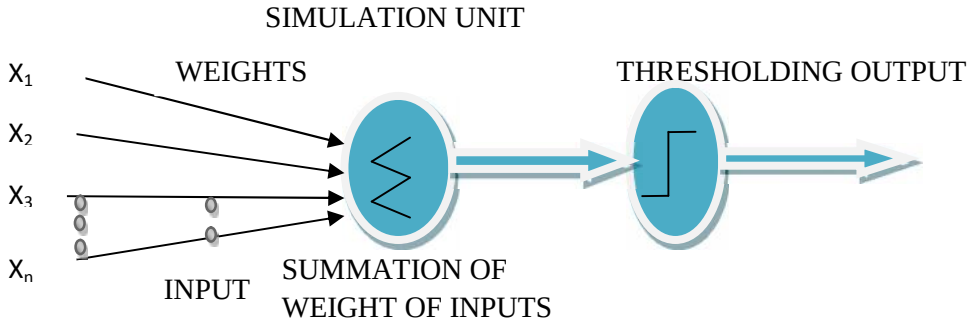

Figure: 5.5 Artificial Neural Network model

Recollect that biological neuron receives all the inputs through the dendrites, sums them and produces an output if the sum is greater than a threshold value. The input signals are passed on to the cell body through the synapse which may accelerate or retard an arriving signal.

It is this acceleration or retardation of the input signals that is modeled by the weights. An effective synapse which transmits a stronger signal will have a correspondingly larger weight while a weak synapse will have smaller weights. Thus, weights here are

multiplicative factors of the input to account for the strength of the synapse. Hence, the total input I received by the soma of the artificial neuron is

$$I = w_1 x_1 + w_2 x_2 + \ldots + w_n x_n \quad (5.3)$$

$$= \sum_{i=1}^{n} w_i x_i \quad (5.4)$$

To generate the final output y, the sum is passed on to a non-linear filter Φ called Activation function, or Transfer function which releases the output.

i.e. $y = c(I)$ (5.5)

The network architecture/ topology or features such as number of neurons and layers are very important factors that determine the functionality and generalization capability of the network. The selection of the activation function and training algorithm also play a significant role to obtain better forecast of response variable. In this work, standard multilayer feed-forward back-propagation hierarchical neural network has been considered for the prediction of erosion wear . The neural network has been designed with **MATLAB** 7.10 software. The back propagation algorithm is a gradient decent error-correcting algorithm which updates the weights in such a way that network output error is minimized. The **feed forward backpropagation** network usually consists of an input layer (where the inputs of the problems are received, the inputs are the activity of collecting data from the relevant sources. These data are fed to the neural network), one hidden layer (where the relationship between the inputs and outputs are established represented by synaptic weights) and an output layer which emits the outputs of the network. The number of hidden layer may vary depending on the nature, complexity and non-linearity of the data at hand, but single hidden layer is sufficient to deal with most of the practical case. In this work, the input layer has three neurons corresponding to each of the parameters and one neurons in the output layer. In order to find out the best network architecture, different networks with different number of hidden layers and neurons in the hidden layer were designed and verified; different training algorithm were used; transfer function in the hidden layer and output layer were changed and observed the generalization capability of the different networks and finally the optimal network was selected to predict tool wear and surface roughness. The issue of determining the optimum

number of hidden nodes is a crucial and complicated one in neuronal model. In general, network with smaller number of hidden neurons are preferable as they usually have better generalizations ability and less over fitting problems. But network with too few hidden neurons may not have enough power to model, store and learn the data. The most common approach in determining the number of hidden neurons (nodes) is via trial and error. Several rule of thumbs have also been proposed, such as, the number of hidden nodes depends on the number of input patterns and each weight should have at least ten input patterns (sample size). In the case of one hidden layer network, several practical guidelines exist. These include 2n+1, 2n, n\2 where n is the number of input nodes. Lawrence and Fredrick suggested that the number of hidden neuron = (n1+n2), where n1 and n2 are the number of input and output nodes respectively.For the optimal network architecture, tangent of sigmoid (sigmoid function is of the form f(x) = (1/1+e-x)) transfer function **'tansig'** has been used in the hidden layer and linear (linear function is of the form f(x) = x)) transfer function **'purelin'** has been used in the output layer**.** The ANN configuration is represented as 3-20-1 that is input layer consists of three input neurons; the hidden layer consists of twenty neurons and the output layer consisting of one output neurons. The number of neurons in the hidden layer is determined by trial and error method after designing and investigating many networks which vary in their structure, transfer function, training algorithm etc. As mentioned above, there is no fixed rule for determining the number of neurons in the hidden layer. The number of neurons in this layer must be large enough to provide non-linear evaluation space in the network.

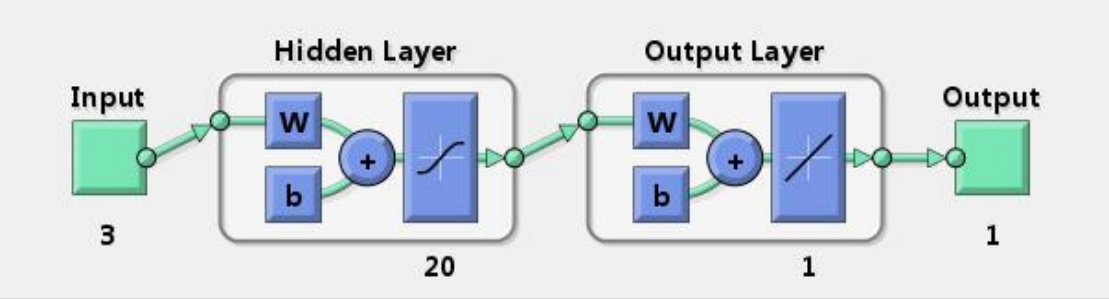

Figure: 5.6 Neural network

The number and size of layers between network inputs and the output layer were determined by testing several combinations of numbers of layers and various numbers of neurons in each layer. Each of the selected combinations was tested with several

different initial conditions to guarantee that the proposed model could provide the best solution.

The accuracy of the prediction depends on how well it has been trained. The training of the neural network using a feed-forward back propagation algorithm has been carried out in the work. The network performs two phases of data flow. First the input information is propagated from the input layer to the output layer and, as a result it produces an output. Then the error signals resulting from the difference between the networks predicted values and the actual values are back propagated from the output layer to the previous layers for them to update their weights accordingly. The update of weights continues until the network error goal is reached.

The number of neurons in the hidden layer is intentionally chosen to start with five neuron and hidden neurons are added to the hidden layer incrementally. The addition of hidden neurons continues until there is no significant progress in network performance. The performance of the network was evaluated by mean squared error (MSE) between the experimental and the predicted values for every output nodes in respect of training the network. The feedback from that processing is called the "average error" or "performance". A training set consists of inputs and the corresponding correct outputs (targets). One of the most powerful learning algorithms, the **Levenberg-Marquardt algorithm** , was used to train the network. In function approximation problems, this algorithm is considered to have the fastest convergence. The input data is converted into normalized form in order to get data in between range of 0.1 to 0.9 using given equation:

$$y = 0.1 + 0.8\left(\frac{x - x_{min}}{x_{max} - x_{min}}\right)$$

Table 5.9 Actual values for input and output variables

Actual Values			Actual values	Actual values	Actual values	Actual values
Speed	Mild Steel	Time	Mild steel	SS202	Coated Mild Steel	Coated SS202
500	39.6	90	39.6	14.3	8.6	6.3
500	72.9	180	72.9	23.8	9.1	9.2
500	52.4	90	52.4	19.8	11.2	9.8
500	99.8	180	99.8	34.8	16.9	14.8
800	64.3	90	64.3	24.7	11.8	10.1
800	124.1	180	124.1	42.2	15.8	17.6
800	111.8	90	111.8	31.1	16.7	15.7
800	211.9	180	211.9	58.1	30.2	27.6
1100	95.9	90	95.9	31.9	15.6	13.4
1100	184.5	180	184.5	59.3	24.9	21.8
1100	151.8	90	151.8	40.2	21.6	19.6
1100	193.8	180	193.8	75.4	38.3	35.5
1400	111.7	90	111.7	36.2	19.1	19.2
1400	217.8	180	217.8	68.6	29.7	27.4
1400	182.7	90	182.7	53.2	26.6	22.5
1400	343.5	180	343.5	99.1	43.1	40.8

Table 5.10 Normalized value for input and output variables

Normalized value			Nor Value	Normalized value	Nor Value	Normalized value
Speed	Concentration	Time	Mild steel	SS202	Coated Mild Steel	Coated SS202
0.1	0.100	0.1	0.100	0.100	0.100	0.100
0.1	0.183	0.9	0.183	0.189	0.111	0.167
0.1	0.137	0.1	0.137	0.151	0.160	0.181
0.1	0.253	0.9	0.253	0.293	0.292	0.297
0.36	0.165	0.1	0.165	0.198	0.174	0.188
0.36	0.322	0.9	0.322	0.363	0.266	0.362
0.36	0.290	0.1	0.290	0.258	0.287	0.317
0.36	0.553	0.9	0.553	0.513	0.600	0.593
0.63	0.248	0.1	0.248	0.266	0.262	0.264
0.63	0.481	0.9	0.481	0.524	0.477	0.459
0.63	0.395	0.1	0.395	0.344	0.401	0.408
0.63	0.505	0.9	0.505	0.676	0.788	0.777
0.9	0.289	0.1	0.289	0.306	0.343	0.399
0.9	0.569	0.9	0.569	0.612	0.589	0.589
0.9	0.476	0.1	0.476	0.466	0.517	0.475
0.9	0.900	0.9	0.900	0.900	0.900	0.900

The training parameters used in shown in Figure. The data sets used were 70% training, 15% validation and 15% testing. The input neuron-hidden layer and output neuron is shown in. Mean square error (MSE) was used for evaluating the performance between experimental and predicted value. The Summary of ANN model is given in Table 10. The algorithm used for the neural network learning is Levenberg- Marquardt (LM) version. Nguyen-Widrow algorithm is used to generate initial weights and values for layer. The percentage error between experimental and ANN model is shown in Table 5.11

Table 5.11 Percentage error between Experimental and ANN model

Mild Steel	ANN	%error	SS202	ANN	%error	Coated Mild Steel	ANN	%error	Coated SS202	ANN	%error
39.6	38.5	2.77	14.3	14.48	1.25	8.6	8.647	0.54	6.3	7.58	20.31
72.9	68.4	6.17	23.8	23.87	0.29	9.1	8.98	1.31	9.2	9.18	0.21
52.4	51.3	2.09	19.8	22.57	13.98	11.2	11.23	0.26	9.8	11.1	13.26
99.8	98.9	0.90	34.8	35.76	2.75	16.9	23.8	17.1	14.8	14.79	0.06
64.3	78.4	21.92	24.7	24.63	0.283	11.8	11.67	1.101	10.1	11.9	17.82
124.1	123.8	0.24	42.2	42.17	0.071	15.8	15.51	1.835	17.6	17.59	0.056
111.8	112.5	0.62	31.1	20.97	22.92	16.7	16.74	0.239	15.7	15.65	0.31
211.9	204.8	3.35	58.1	58.16	0.103	30.2	29.9	0.993	27.6	27.56	0.14
95.9	125.8	20.75	31.9	31.6	0.940	15.6	15.42	1.153	13.4	13.37	0.22
184.5	184.3	0.10	59.3	59.28	0.033	24.9	24.82	0.321	21.8	21.78	0.09
151.8	151.6	0.13	40.2	33.8	15.92	21.6	17.31	19.86	19.6	19.58	0.10
193.8	193.4	0.20	75.4	88.56	17.45	38.3	39.77	3.838	35.5	35.49	0.02
111.7	111.3	0.35	36.2	36.13	0.193	19.1	18.98	0.628	19.2	19.1	0.52
217.8	216.8	0.45	68.6	68.63	0.043	29.7	29.64	0.202	27.4	26.92	1.75
182.7	175.1	4.15	53.2	53.09	0.206	26.6	21.89	17.70	22.5	22.44	0.26
343.5	342.8	0.20	99.1	98.1	1.009	43.1	42.94	0.371	40.8	39.8	2.45

5. 4. 2 LEARNING METHODS FOR ANN

GRADIENT DESCENT LEARNING

This is based on the minimization of error *E* defined in terms of weights and the activation functions of the network. Also, it is required that the activation function employed by the network is differentiable, as the weight update is dependent on the gradient of the error *E*.

Thus, if ΔW_{ij} is the weight update of the link connecting the *i*th and *j*th neuron of the two neighbouring layers, then ΔW_{ij} is defined as

$$\Delta Wij = \eta \frac{\partial E}{\partial w_{ij}}$$

Where, η is the learning rate parameter and $\frac{\partial E}{\partial w_{ij}}$ is the error gradient with reference to the weight W_{ij}..The widrow and Hoffs Delta rule and Back propagation learning rule are all examples of this type of learning mechanism.

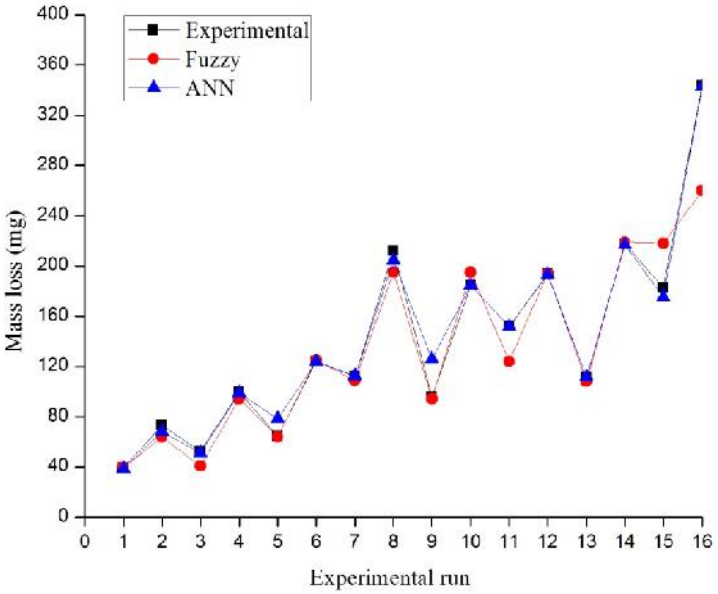

Figure: 5.7 Graph between experimental and predicted values

The graph between experimental and predicted values for mild steel shows that the average percentage error between experimental and fuzzy logic values is 7.7% while the average error between experimental and ANN values is 4.024%.

CHAPTER 6 CONCLUSIONS AND FUTURE SCOPE

6.1 CONCLUSIONS

Investigations of the parameters affecting the erosion wear of slurry pipeline materials and coatings have been carried out in the present work using slurry pot tester. Fuzzy logic and ANN technique has been implemented for the study of erosion performance under various test conditions. The coating on the base material is deposited using Atmospheric Plasma spraying.

1. The erosion resistance of SS202 is maximum under all circumstances.

2. The coated specimen showed approximated 2-3 times better erosion resistance as compared to uncoated specimen.

3. The erosion mechanism exhibited by Al_2O_3 + 13% TiO_2 is brittle in nature with grain pull out, grain dislodgment and micro cutting as major mechanism. Major cause of micro fracture in Alumina titania coating is due dislocation pile up against grain boundaries that in turn triggers grain pull out.

4. The speed and concentration exponent for erosion rate is in correlation with the previous researchers.

5. The predicted values by Fuzzy logic and ANN were approximated close with average percentage error of 7 to 8 % and 4 to 5 % respectively.

6.2 SCOPE FOR FUTURE WORK

Different variables like impact angle, different erodent etc can also be used to study the erosion performance of slurry pipelines. Various erosion tester can also be used to determine the improvement in erosion wear results. Coating parameters can be more optimized to improve the coating hardness and other coating materials can be used to improve the erosion wear resistance. Computational Fluid dynamics can also be applied for simulation of erosion wear with different operating parameters.

REFERENCES

[1]. Soo S.L (1967)., "Fluid Dynamics of Multiphase Systems", Blaisdell, Waltham, MA

[2]. Truscott G.F., (1975) "A literature Survey on Wear on Pipelines", BHRA Fluid Engineering, *Cranfield Publ.*, Cranfield, UK, TN 1295.

[3]. Shin Y.C., and Vishnupad P., (1996) " Neuro-Fuzzy Control of Complex Manufacturing Processes, " *International Journal of Production Research,* 34(12): 291-330

[4]. Fuzzy control programming. Technical Report (1997)"*International Electrotechnical Commision"*

[5]. Mahapatra S.S., and Patnaik Amar., (2009), "Study on mechanical and erosion wear behaviour of hybrid composities using Taguchi experimental design", *Materials and Design,* 30(2): 2791- 2801.

[6]. Mishra S.K., and Patnaik A., (2012), "Erosion wear analysis of Al_2O_3 particles reinforced with ZA-27 Alloy Metal Matrix Composite using ANN", *Academics research journal,* 1: 65-76

[7]. Pati P.R., and Satapathy A., (2013), " Prediction and Simulation of Erosion Wear Response of Linz- Donawitz slag filled epoxy composites using ANN", *International Journal on Mechanical Engineering and Robotics,* 1(1): 39-45

[8]. Grewal H.S., Agrawal A. and Singh H., (2013), "Slurry Erosion Mechanism of Hydroturbine Steel: Effect of Operating Parameters", *Tribology Letters,* 52(2): 287-303.

[9]. Torres M.V., Camacho J.R., Castillo R.E., Hernandez E.A., Cardenas E.E. and Torres J.V., (2013), "Study of solid particle erosion on AISI 420 stainless steel using angular silicon carbide and steel round grit particles", *Wear,* 301(1-2): 383-389.

[10]. Grewal H.S., Agrawal A., Singh H. and Shollock B.A., (2014), "Slurry Erosion Performance of Ni-Al2O3 Based Thermal-Sprayed Coatings: Effect of Angle of Impingement", *Journal of Thermal Spray Technology,* 23(3): 389-401.

[11]. Sridhar R., Murthy H.N.N., Krishna M., (2014), " Effect of Nanoclay Addition on the Erosion Wear of Glass/vinylester Composites Using Taguchi's Orthogonal Array Technique", *Procedia Materials Science,* 50 (2): 1174-1181

[12]. Andrews N., Giourntas L., GallowayA.M. and Pearson A., (2014), "Effect of impact angle on the slurry erosion-corrosion of Stellite 6 and SS316", *Wear,* 320 (1-2): 143-151

[13]. Elrhman Y.M., Kasem A.A., Emara K.M. and Ahmed S.M, (2013), "Effect of impact angle on slurry erosion behavior and mechanism of carburized AISI 5117 steel", *Journal of Tribology,*136(1): 011106.

[14]. Paul C.P., Gandhi B.K., Bhargawa P., Dwivedi D.K. and Kukreja L.M., (2014), "Cobalt-Free Laser Cladding on AISI Type 316L Stainless Steel for Improved Cavitation and Slurry Erosion Wear Behavior", *Journal of Materials Engineering and Performance,*23(12): 4463-3371

[15]. Singh H., Goyal K. and Goyal D.K., (2014), "Slurry Erosion Behaviour of Plasma Thermal Sprayed (50%) WC-Co-Cr and Ni-Cr-B-Si Coatings of Different Thickness on CA6NM Turbine Steel Material", *Manufacturing Science and Technology,* 2(4): 81-92.

[16]. Lotfollahi M., Shamanian M. and Saatchi A., (2014), "Effect of friction stir processing on erosion–corrosion behavior of nickel–aluminum bronze", *Material And Design,* 62: 282-287

[17]. Singh Prabhjot., (2014), "Investigation of Slurry Erosion in pipeline materials", Mtech Thesis, Thapar University, Patiala, India

[18]. Joshi A.G., Kumar M.P and Basavarajappa S., (2014), "Influence of Al_2O_3 Filler on Slurry Erosion Behavior of Glass/Epoxy Composites", *International Conference on Advances in Manufacturing and Material Engineering, AMME 2014,* 5: 863-872.

[19]. Goyal D.K., Singh H., Kumar H. and Sahni V., (2014), "Erosive Wear Study of HVOF Spray Cr3C2–NiCr Coated CA6NM Turbine Steel", *Journal of Tribology,* 136(4):041602.

[20]. Islam Md. A and Farhat Z.N., (2014), "Effect of impact angle and velocity on erosion of API X42 pipeline steel under high abrasive feed rate", *Wear,* 311(1-2): 180-190.

[21]. Lindgren M. and Perolainen J., (2014), “Slurry pot investigation of the influence of erodent characteristics on the erosion resistance of austenitic and duplex stainless steel grades”, *Wear,* 319(1-2): 38-48.

[22]. Lindgren M. and Perolainen J., (2014), “Slurry pot investigation of the influence of erodent characteristics on the erosion resistance of titanium”, *Wear,* 321: 64-69.

[23]. Nguyen Q.B., Nguyen V.B., Lim C.Y.M., Sankaranarayanan S., Zhang Y.W. and Gupta M., (2014), “Effect of impact angle and testing time on erosion of stainless steel at higher velocities”, *Wear,* 321: 87-93.

[24]. Ji W.W., Guo Z., Tang L. and Du H., (2014), “Degradation process of typical Ti(C,N)–Mo2C–Ni cermet in slurry erosion conditions”, *Tribilogy International,* 74:138-144.

[25]. Andrews N., Giourntas L., GallowayA.M. and Pearson A., (2015), “Erosion–corrosion behaviour of zirconia, WC–6Co,WC–6Ni and UNS S31600”, *International Journal of Refractory metals and Hard Material,* 48: 229-237.

[26]. Ren Z.H., Jin P., Cao X.M., Zheng Y.G. and Zhang J.S., (2015), “Mechanical properties and slurry erosion resistance of SiC ceramic foam/epoxy co-continuous phase composite”, *Composites Science and Technology,* 107: 129-136.

[27]. Lindgren M., Suihkonen R., Vuorinen J., (2015), “Erosive wear of various stainless steel grades used as impeller blade materials in high temperature aqueous slurry”, *Wear,* 328-329: 391-400.